

# eIF5B gates the transition from translation initiation to elongation

Jinfan Wang<sup>1</sup>, Alex G. Johnson<sup>1,2</sup>, Christopher P. Lapointe<sup>1</sup>, Junhong Choi<sup>1,3</sup>, Arjun Prabhakar<sup>1,4</sup>, Dong-Hua Chen<sup>1</sup>, Alexey N. Petrov<sup>1,5</sup> & Joseph D. Puglisi<sup>1\*</sup>

**Translation initiation determines both the quantity and identity of the protein that is encoded in an mRNA by establishing the reading frame for protein synthesis. In eukaryotic cells, numerous translation initiation factors prepare ribosomes for polypeptide synthesis; however, the underlying dynamics of this process remain unclear<sup>1,2</sup>. A central question is how eukaryotic ribosomes transition from translation initiation to elongation. Here we use in vitro single-molecule fluorescence microscopy approaches in a purified yeast *Saccharomyces cerevisiae* translation system to monitor directly, in real time, the pathways of late translation initiation and the transition to elongation. This transition was slower in our eukaryotic system than that reported for *Escherichia coli*<sup>3–5</sup>. The slow entry to elongation was defined by a long residence time of eukaryotic initiation factor 5B (eIF5B) on the 80S ribosome after the joining of individual ribosomal subunits—a process that is catalysed by this universally conserved initiation factor. Inhibition of the GTPase activity of eIF5B after the joining of ribosomal subunits prevented the dissociation of eIF5B from the 80S complex, thereby preventing elongation. Our findings illustrate how the dissociation of eIF5B serves as a kinetic checkpoint for the transition from initiation to elongation, and how its release may be governed by a change in the conformation of the ribosome complex that triggers GTP hydrolysis.**

Despite decades of study, the transition from translation initiation to elongation in eukaryotes remains poorly understood. During translation initiation, the 40S ribosome subunit in complex with initiation factors is recruited to a 7-methylguanosine (m<sup>7</sup>G)-capped mRNA and scans the 5' untranslated region until the correct AUG start codon is recognized (termed 'scanning'), at which point a post-scanning 48S pre-initiation complex (PIC) is formed<sup>1,2</sup>. The subsequent joining of the 60S subunit to this 48S PIC is catalysed by the universally conserved factor eIF5B, independently of its GTPase activity<sup>6–9</sup>. The conformation of yeast eIF5B when bound to GTP is remodelled after association with a ribosome, and this conformational change enables eIF5B to contact directly both Met-tRNA<sup>Met</sup> and the GTPase activation centre on the 60S subunit<sup>10–12</sup>. These contacts are probably essential for triggering the hydrolysis of GTP and the subsequent release of eIF5B-GDP, which allows the ribosomal A site to accept the first elongator aminoacyl-tRNA (aa-tRNA) and enter the elongation phase<sup>12</sup>. Bypassing the hydrolysis of GTP by eIF5B with a mutation that weakens the ribosome-binding affinity of the factor increases the frequency of the first AUG codon in an mRNA being bypassed ('leaky scanning') in vivo<sup>8</sup>—which implies that the timing of the dissociation of eIF5B from the 80S complex and the subsequent entry into elongation is critical to start-site selection. The steps that govern this transition—and their timescales—have not been elucidated in eukaryotes because the complex, multi-step nature of the transition challenges traditional biochemical approaches.

Here we overcome these limitations by using single-molecule fluorescence microscopy to observe translation initiation directly, and thereby elucidate the dynamics and pathways that are involved in the assembly of the 80S complex and subsequent acceptance of the first

elongator aa-tRNA. We first reconstituted an active yeast translation system from purified ribosomes and core eukaryotic initiation and elongation factors (Extended Data Fig. 1) that is suitable for single-molecule analyses<sup>13</sup>. We then applied this system to study the assembly of the 80S complex in real time using a zero-mode waveguide (ZMW)-based instrumentation platform<sup>14</sup>, which is capable of multi-colour single-molecule fluorescence imaging at high concentrations of fluorescently labelled ligands.

Given that we observed efficient and stable formation of the 48S PIC on an uncapped, unstructured model mRNA that has been well-characterized previously<sup>9</sup> (Fig. 1a, Extended Data Fig. 2a), we formed and immobilized single 48S PICs (containing the cyanine 3-labelled 40S subunit, Cy3-40S) within ZMWs and delivered Cy5-60S along with the other required factors (Extended Data Fig. 3a). We observed efficient joining of the 60S subunit on single 48S PICs—around 90% ( $n = 267$  out of 300) of the 48S PICs bound to Cy5-60S to form the 80S complex (Extended Data Fig. 3b, c). This required eIF5B; in the absence of eIF5B, no 80S formation was observed in the 15-min time window that was used for imaging ( $n = 500$ ); of note, yeast that lack eIF5B are able to survive (albeit with a severe growth defect<sup>8</sup>) despite the critical role of this factor, which may be because the presence of polyamines can lead to functional subunit joining in the absence of eIF5B (Extended Data Fig. 3d, e). The association rate of 60S subunits was comparable to that from previous bulk measurements<sup>9</sup> (Extended Data Fig. 3c). When we labelled the first elongator Phe-tRNA<sup>Phe</sup> with Cy3.5 and included this in the delivery mix as a ternary complex with eukaryotic elongation factor 1A (eEF1A) and GTP (Cy3.5-Phe-TC) (Fig. 1b), around 80% ( $n = 164$  out of 200) of the 60S joining events (signalled by single-molecule fluorescence resonance energy transfer, smFRET) were followed by a subsequent Cy3.5-Phe-TC arrival event (Fig. 1c). This association of aa-tRNA with the ribosomal A site was codon- and tRNA-specific and led to further elongation (Extended Data Fig. 4). These results demonstrate that real-time 80S assembly occurs in the correct reading frame and that our single-molecule system for translation initiation is fully active.

To determine an initial rate for the transition from initiation to elongation, we measured the dwell times between 60S joining and the arrival of Cy3.5-Phe-TC, and determined the average time of this transition ( $\Delta t$ ) (Fig. 1c). The  $\Delta t$  value was  $30.2 \pm 1.0$  s ( $n = 147$ ) ( $\pm 95\%$  confidence interval) when assayed under the same conditions as were used in previous bulk kinetic analyses of yeast translation initiation<sup>9</sup> (26 °C and buffer containing 3 mM free Mg<sup>2+</sup>). This is substantially longer than that in bacterial translation, for which the  $\Delta t$  value was reported to be approximately 1 s at 20 °C<sup>3–5</sup>. For direct comparisons with the bacterial rates, we also determined the  $\Delta t$  value at 20 °C ( $92.2 \pm 2.5$  s) (Fig. 1d). The  $\Delta t$  value remained similar after addition of 150 nM eIF3 and 200 nM eEF3 (and 1 mM ATP:Mg<sup>2+</sup>) or addition of 500 nM hypusine-modified eIF5A<sup>15</sup>—indicating that the transition from initiation to elongation is independent of these factors (Extended Data Fig. 5a). Changing the concentration of Cy3.5-Phe-TC did not

<sup>1</sup>Department of Structural Biology, Stanford University School of Medicine, Stanford, CA, USA. <sup>2</sup>Department of Chemical and Systems Biology, Stanford University School of Medicine, Stanford, CA, USA. <sup>3</sup>Department of Applied Physics, Stanford University, Stanford, CA, USA. <sup>4</sup>Program in Biophysics, Stanford University, Stanford, CA, USA. <sup>5</sup>Present address: Department of Biological Sciences, Auburn University, Auburn, AL, USA. \*e-mail: puglisi@stanford.edu



**Fig. 1 | Real-time observation of eukaryotic translation initiation and the transition to elongation.** **a**, mRNA constructs used in single-molecule assays (Extended Data Fig. 5d). All of the mRNAs contain a UUC Phe codon after the AUG start codon and are biotinylated at their 3'-ends. p, phosphate group; nt, nucleotide. **b**, Experimental setup for single-molecule assays. 48S PICs containing Cy3-40S, Met-tRNA<sup>Met</sup><sub>1</sub> and the 3'-end-biotinylated mRNA of interest were immobilized in ZMWs in the presence of the required initiation factors (eIFs). Experiments were started by illuminating ZMWs with a green laser and delivering Cy5-60S, Cy3.5-Phe-TC and initiation factors. **c**, Example experimental trace (bottom) and schematic (top) of the molecular events along the reaction coordinate. IC, initiation complex; EC, elongation complex. **d**, The dwell times between the 60S joining and the arrival of Phe-TC to the A site were measured and fitted to single-exponential distributions to estimate the average time,  $\Delta t$ , of the transition from initiation to elongation. For bars from bottom to top:  $n = 118$ ,  $n = 130$ ,  $n = 130$ ,  $n = 121$ ,  $n = 189$ ,  $n = 159$ ,  $n = 164$  and  $n = 136$  molecules. Error bars show 95% confidence intervals.

notably alter the  $\Delta t$  value (Extended Data Fig. 5b). Thus, the rate of the transition is limited by a step that occurs before binding of the first aa-tRNA to the A site.

We next questioned whether the slow transition was a result of the m<sup>7</sup>G-cap-independence of initiation on the model mRNA (that is, the lack of the m<sup>7</sup>G cap on the model mRNA and eIF4F proteins in the reaction). We formed 48S PICs on *RPL41A* or *RPL30* mRNAs that were completely capped with m<sup>7</sup>G (cap-*RPL41A* or cap-*RPL30*, respectively) (Fig. 1a, Methods) in the presence of eIF4F, eIF4B and eIF3 proteins and performed the same experiments as above. The 48S PICs readily formed in a cap-dependent manner (Extended Data Fig. 2b), and cryo-electron microscopy (cryo-EM) analyses of the complexes showed that they were in the post-scanning, mRNA-channel-'closed' state<sup>16</sup> (Extended Data Fig. 2c–e). Thus, the 48S PIC that was central to our single-molecule assays is an authentic and on-pathway complex. However, the  $\Delta t$  values at 20 °C were  $81.4 \pm 2.5$  s and  $65.7 \pm 3.4$  s for cap-*RPL41A* and cap-*RPL30*, respectively—similar to the  $\Delta t$  value that was measured on the model mRNA (Fig. 1d). Increasing the Cy3.5-Phe-TC concentration did not markedly change the  $\Delta t$  value (Extended Data Fig. 5c), which further demonstrates that the rate-limiting step occurs before aa-tRNA binding to the A site. Our findings suggest that the slow transition to elongation may be a general feature of yeast translation.

We next tested whether the sequence context near the start codon affected entry into the elongation phase of translation. When the optimal yeast Kozak sequence<sup>17</sup> was inserted upstream of the AUG codon in the model mRNA (designated as model mRNA-Kozak), the  $\Delta t$  value was reduced by around threefold to  $34.1 \pm 1.3$  s at 20 °C (Fig. 1a, d). This effect was largely abolished by an A to U substitution at the -3 position (Extended Data Fig. 5d), consistent with the critical role of that residue within the Kozak sequence<sup>18</sup>. We have thus uncovered a role of the Kozak sequence in the control of this transition. However, even the fastest rate we observed at 20 °C was still more than 30-fold slower than that observed in *E. coli*<sup>3–5</sup>. To understand the energetics of the rate-limiting step in the eukaryotic transition,

we increased the reaction temperature to 30 °C (which is within the optimal temperature range for growth of *S. cerevisiae*<sup>19</sup>), and found that  $\Delta t$  depended on temperature across all assayed mRNAs (Fig. 1d, Extended Data Fig. 5d). At 30 °C, the  $\Delta t$  value decreased by approximately 4–5-fold compared to the value at 20 °C for the model, cap-*RPL41A* and cap-*RPL30* mRNAs, and by around 2.5-fold for the model mRNA-Kozak.

The temperature dependence of the  $\Delta t$  value suggested that slow conformational rearrangements and/or factor dissociation that are predominantly driven by changes in enthalpy limited the transition. We hypothesized that dissociation of eIF5B was the rate-limiting step, given that its binding site on the ribosome overlaps with that of the elongator aa-tRNAs<sup>12</sup>. Previous kinetic analyses of translation in rabbit reticulocyte lysate suggest that GTP hydrolysis by an initiation factor limits the rate at which the first peptide bond is formed after the joining of ribosomal subunits<sup>20</sup>. This GTP hydrolysis could plausibly be that by eIF5B. If eIF5B indeed gates the transition to elongation, we would expect its lifetime on the 80S complex to be similar to the  $\Delta t$  values that we measured above.

To test this hypothesis, we fluorescently labelled eIF5B (Extended Data Fig. 6a) and tracked the protein throughout the reaction pathways using a similar experimental scheme as above. A Cy5.5 dye was attached to N-terminally truncated eIF5B (remaining residues 396–1002) through a ybbR tag fused to the N terminus. Note that this truncated eIF5B is the standard construct in the eukaryotic translation field<sup>6,9,21,22</sup>; it was used in all of our measurements above that involved eIF5B (Extended Data Fig. 6b) and neither the tag nor the dye affected the function of eIF5B (Extended Data Fig. 6c, d). After immobilizing pre-formed Cy3-48S PICs in ZMWs, we co-delivered Cy5.5-eIF5B, Cy5-60S and Cy3.5-Phe-TC to the immobilized complexes in the presence of other required factors. With the model mRNA and direct illumination of all fluorophores, we observed transient sampling events of Cy5.5-eIF5B to the 48S PIC before 60S joining (mean lifetime =  $0.59 \pm 0.06$  s,  $n = 903$  events; Extended Data Fig. 7a), which is consistent with the dynamic interaction of eIF5B with the 48S PIC that has been suggested by previous measurements with ensemble fluorescence approaches<sup>9</sup>. After the joining of Cy5-60S to form the 80S complex (as shown by the smFRET signal), the average lifetime of Cy5.5-eIF5B on the ribosome was prolonged and nearly equal to  $\Delta t$  (Fig. 2a–c, Extended Data Fig. 7a). The  $\Delta t$  value measured here matched that measured with unlabelled eIF5B, which confirms that labelling did not affect eIF5B function (Extended Data Fig. 6e). Furthermore, dissociation of Cy5.5-eIF5B always preceded the binding of Cy3.5-Phe-TC to the A site of the 80S ribosome, which occurred very rapidly (within 1 s) after eIF5B departure (Fig. 2a, d). Similar results were observed for all mRNAs at both 20 °C and 30 °C (Fig. 2c). Notably, the  $\Delta t$  value was not reduced by using full-length eIF5B, which indicates that the lack of the non-conserved N-terminal region<sup>8,10</sup> of the protein did not interfere with the transition rate (Extended Data Fig. 6b, f, g). Thus, the presence of eIF5B on the de novo-assembled 80S ribosome limits the rate of the transition from initiation to elongation.

We hypothesize that the rate of GTP hydrolysis by eIF5B defines its residence time on the 80S complex. The  $\Delta t$  value that was measured here on the model mRNA was similar to the mean time of GTP hydrolysis by eIF5B during initiation on the same type of model mRNA (approximately 30.2 s versus 28 s at 26 °C)<sup>21</sup>. Notably, inclusion of a non-hydrolysable GTP analogue (GDPNP) trapped eIF5B on the 80S complex (average Cy5.5-eIF5B lifetime on the 80S was around 850 s and was limited by photobleaching and imaging time;  $n = 105$ ), and prevented the association of aa-tRNA with the ribosomal A site (Extended Data Fig. 7b, c). To further investigate this finding, we used two previously reported mutant versions of eIF5B that exhibit disrupted GTPase activity<sup>8</sup>. In the first of these mutants (eIF5B(T439A)), tRNA association with the A site was inhibited (only 17 out of 131 assembled 80S ribosomes underwent A-site tRNA association) and the  $\Delta t$  value increased to around 370 s at 20 °C (Extended Data Fig. 8). By contrast, in the second mutant (eIF5B(H505Y)), which also has weakened

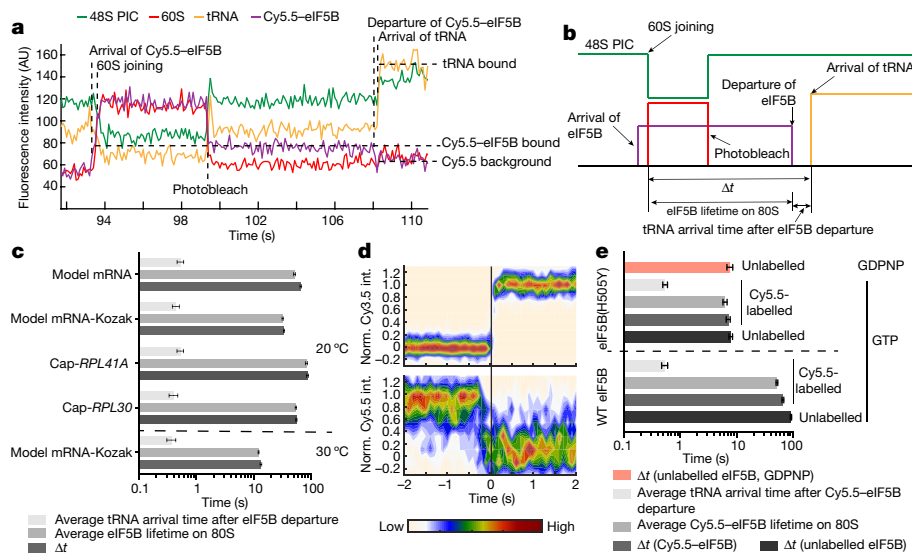


**Fig. 2 | eIF5B gates the transition between initiation and elongation.**

**a, b**, Sample trace (**a**) and schematic (**b**) showing the correlation of Cy5.5–eIF5B occupancy on the ribosomal complex with Cy5–60S joining and the arrival of Cy3.5–Phe–TC. **c**, For all assayed mRNAs, the  $\Delta t$  value, average eIF5B lifetime on 80S and average tRNA arrival time after eIF5B departure were estimated by fitting the dwell times to single-exponential distributions (Extended Data Fig. 9g). From bottom to top for each group of three bars:  $n = 141$ ,  $n = 164$ ,  $n = 133$ ,  $n = 131$  and  $n = 134$  molecules. Error bars show 95% confidence intervals. **d**, Contour plots of the departure of Cy5.5–eIF5B (bottom; normalized Cy5.5 fluorescence intensity (norm. Cy5.5 int.) changing from 1 to 0) and the arrival of Cy3.5–Phe–TC (top; normalized Cy3.5 intensity (norm. Cy3.5 int.))

affinity for the ribosome, the  $\Delta t$  value decreased by about 15-fold ( $n = 119$ ) compared to wild-type eIF5B (Fig. 2e, Extended Data Fig. 8). The H505Y mutation instead reduced the occupancy time of eIF5B on the ribosome compared to wild type independent of GTP hydrolysis (Fig. 2e). Thus, eIF5B departure is indeed controlled by GTP hydrolysis.

The marked dependence of the eIF5B departure rate from the 80S complex on temperature and on the concentration of free  $Mg^{2+}$  (Extended Data Fig. 9) suggests that the GTP hydrolysis activity of eIF5B is sensitive to the conformation of the ribosome. We therefore applied cryo-EM, guided by our single-molecule kinetics, to analyse the conformations of on-pathway ribosomal complexes that were assembled in the presence of wild-type eIF5B and GTP. We added eIF5B–GTP and 60S subunits to assembled 48S PICs (on the model mRNA) (Fig. 1a) and allowed the reaction to proceed at about 20°C for 45 s (from mixing to grid plunge-freezing) (Methods), which corresponds to a pre-steady-state time point according to our single-molecule measurements (Extended Data Fig. 10a, Methods). Two distinct classes of 80S complexes were resolved: (1) the eIF5B-bound 80S initiation complex; and (2) the 80S elongation complex (Extended

changing from 0 to 1) in experiments performed with model mRNA in the presence of GTP. Plots were generated by superimposing all the analysed fluorescence traces such that the time point of Cy3.5–Phe–TC arrival was set at 0. Contours are plotted from tan (lowest population) to red (highest population);  $n = 134$ . **e**, The same types of average dwell times as in **c** were determined for experiments performed with the model mRNA in the presence of 3 mM free  $Mg^{2+}$  at 20°C. Experiments were performed either in the presence of GTP with unlabelled wild-type (WT) eIF5B ( $n = 164$ ; data taken from Fig. 1d), Cy5.5-labelled wild-type eIF5B ( $n = 134$ ; data taken from **c**), unlabelled eIF5B(H505Y) ( $n = 119$ ) or Cy5.5-labelled eIF5B(H505Y) ( $n = 80$ ); or separately in the presence of GDPNP with unlabelled eIF5B(H505Y) ( $n = 80$ ) (Extended Data Fig. 9h).

Data Fig. 10c, d). The two states were populated in agreement with predictions from our single-molecule kinetics (Extended Data Fig. 10a, b). Similar to that of the reported 80S complex bound to eIF5B–GDPNP<sup>12</sup>, the eIF5B-bound 80S initiation complex (class 1) adopts a semi-rotated inter-subunit conformation, with the Met–tRNA<sup>Met</sup><sub>i</sub> in the 80S peptidyl/initiation configuration. Moreover, eIF1A density was absent in this complex. Its dissociation therefore occurs before the departure of eIF5B and is not the rate-limiting step<sup>9</sup>. After dissociation of eIF5B, the 80S initiation complex matured to the 80S elongation complex (class 2) in a non-rotated-state, with Met–tRNA<sup>Met</sup><sub>i</sub> shifted to the 80S peptidyl/peptidyl configuration—poising the ribosome for rapid association of tRNA with the A site. Together, we propose that the irreversible hydrolysis of GTP by eIF5B and its subsequent dissociation serves as a final kinetic quality-control checkpoint of the assembly of the 80S complex before entry into the energy-expensive elongation phase.

In summary, we have demonstrated that in *S. cerevisiae* (and probably in other eukaryotic systems<sup>20</sup>), eIF5B gates the transition from translation initiation to elongation (Fig. 3). The shortest transition time that we measured in m<sup>7</sup>G-cap-dependent translation was approximately

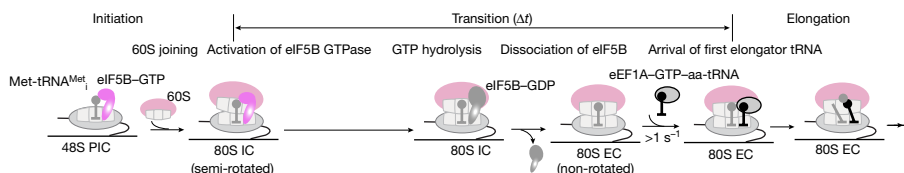


**Fig. 3 | Model of the late events of eukaryotic translation initiation and the transition to elongation.** eIF5B catalyses the joining of the 60S subunit to the 48S PIC to form the 80S initiation complex (80S IC). Dissociation of eIF5B from the 80S initiation complex requires the hydrolysis of GTP, and this plausibly leads to a change in the conformation of eIF5B that lowers its affinity for the 80S. Thus, the dissociation of eIF5B from the 80S initiation complex gates the transition to elongation, which

is marked by the binding of an elongator aa-tRNA to the 80S elongation complex (80S EC). The effects of free  $Mg^{2+}$  concentration, temperature and the sequence context that surrounds the start codon on the rate of the transition indicate that conformational rearrangements may have key roles in governing the rate of eIF5B dissociation, probably by controlling its GTPase activity.



8 s (in the presence of 2 mM free  $Mg^{2+}$  at 30 °C) (Extended Data Fig. 9b)—a timescale that is relevant to the estimated rates of translation initiation in yeast *in vivo* (which vary from several seconds to minutes at 30 °C)<sup>23,24</sup>. The transition to elongation is probably gated by the hydrolysis of GTP by eIF5B, as shown by the correspondence between the rate of GTP hydrolysis<sup>21</sup> and the occupancy time of eIF5B on the 80S complex, and by our observation that the 80S complex bound to eIF5B (probably with GTP) is in a similar conformation to that observed for non-hydrolysable GTP<sup>12</sup>. We speculate that the long lifetime of eIF5B-bound 80S complexes could partially account for the enrichment of ribosome-protected mRNA fragments at the start codon that has been observed in ribosome profiling experiments in eukaryotic systems<sup>25–27</sup>. The relatively slow transition between translation initiation and elongation in the eukaryotic system compared with the bacterial counterpart provides a mechanism to control the density of ribosomes in the early part of the mRNA open reading frame<sup>23,28</sup> to prevent ribosome collisions<sup>29,30</sup>, and a final kinetic checkpoint for accurate start-codon selection. Consistent with the latter proposal, disruption of GTPase activity results in a higher propensity for leaky scanning *in vivo*<sup>8</sup>, and the residence time of eIF5B on the 80S is strongly dependent on the sequence context that surrounds the start codon, with non-optimal Kozak sequences leading to longer residence times. Subtle conformational signalling—perhaps through the initiator tRNA—may modulate the final conformation of the 80S–eIF5B complex for rapid hydrolysis of GTP and subsequent formation of an elongation-competent 80S complex. Finally, we expect that there are many kinetic checkpoints in the early stages of eukaryotic translation. The application of similar single-molecule approaches will unveil the complicated dynamics that underlie mRNA selection, scanning and start-codon selection and the mechanisms by which they are regulated<sup>1,2</sup>.

### Online content

Any methods, additional references, Nature Research reporting summaries, source data, extended data, supplementary information, acknowledgements, peer review information; details of author contributions and competing interests; and statements of data and code availability are available at <https://doi.org/10.1038/s41586-019-1561-0>

Received: 22 February 2019; Accepted: 13 August 2019;

Published online 18 September 2019.

- Hinnebusch, A. G. The scanning mechanism of eukaryotic translation initiation. *Annu. Rev. Biochem.* **83**, 779–812 (2014).
- Sokabe, M. & Fraser, C. S. Toward a kinetic understanding of eukaryotic translation. *Cold Spring Harb. Perspect. Biol.* **11**, a032706 (2019).
- Kaledhonkar, S. et al. Late steps in bacterial translation initiation visualized using time-resolved cryo-EM. *Nature* **570**, 400–404 (2019).
- Tsai, A. et al. Heterogeneous pathways and timing of factor departure during translation initiation. *Nature* **487**, 390–393 (2012).
- Goyal, A., Belardinelli, R., Maracci, C., Milón, P. & Rodnina, M. V. Directional transition from initiation to elongation in bacterial translation. *Nucleic Acids Res.* **43**, 10700–10712 (2015).
- Pestova, T. V. et al. The joining of ribosomal subunits in eukaryotes requires eIF5B. *Nature* **403**, 332–335 (2000).
- Lee, J. H. et al. Initiation factor eIF5B catalyzes second GTP-dependent step in eukaryotic translation initiation. *Proc. Natl Acad. Sci. USA* **99**, 16689–16694 (2002).
- Shin, B. S. et al. Uncoupling of initiation factor eIF5B/IF2 GTPase and translational activities by mutations that lower ribosome affinity. *Cell* **111**, 1015–1025 (2002).
- Acker, M. G. et al. Kinetic analysis of late steps of eukaryotic translation initiation. *J. Mol. Biol.* **385**, 491–506 (2009).
- Roll-Mecak, A., Cao, C., Dever, T. E. & Burley, S. K. X-ray structures of the universal translation initiation factor IF2/eIF5B: conformational changes on GDP and GTP binding. *Cell* **103**, 781–792 (2000).
- Kuhle, B. & Ficner, R. eIF5B employs a novel domain release mechanism to catalyze ribosomal subunit joining. *EMBO J.* **33**, 1177–1191 (2014).
- Fernández, I. S. et al. Molecular architecture of a eukaryotic translational initiation complex. *Science* **342**, 1240585 (2013).
- Acker, M. G., Koltz, S. E., Mitchell, S. F., Nanda, J. S. & Lorsch, J. R. Reconstitution of yeast translation initiation. *Methods Enzymol.* **430**, 111–145 (2007).
- Chen, J. et al. High-throughput platform for real-time monitoring of biological processes by multicolor single-molecule fluorescence. *Proc. Natl Acad. Sci. USA* **111**, 664–669 (2014).
- Gutiérrez, E. et al. eIF5A promotes translation of polyproline motifs. *Mol. Cell* **51**, 35–45 (2013).
- Llácer, J. L. et al. Conformational differences between open and closed states of the eukaryotic translation initiation complex. *Mol. Cell* **59**, 399–412 (2015).
- Hamilton, R., Watanabe, C. K. & de Boer, H. A. Compilation and comparison of the sequence context around the AUG startcodons in *Saccharomyces cerevisiae* mRNAs. *Nucleic Acids Res.* **15**, 3581–3593 (1987).
- Li, J. J., Chew, G. L. & Biggin, M. D. Quantitating translational control: mRNA abundance-dependent and independent contributions and the mRNA sequences that specify them. *Nucleic Acids Res.* **45**, 11821–11836 (2017).
- Walsh, R. M. & Martin, P. A. Growth of *Saccharomyces cerevisiae* and *Saccharomyces uvarum* in a temperature gradient incubator. *J. Inst. Brew.* **83**, 169–172 (1977).
- Lorsch, J. R. & Herschlag, D. Kinetic dissection of fundamental processes of eukaryotic translation initiation *in vitro*. *EMBO J.* **18**, 6705–6717 (1999).
- Acker, M. G., Shin, B. S., Dever, T. E. & Lorsch, J. R. Interaction between eukaryotic initiation factors 1A and 5B is required for efficient ribosomal subunit joining. *J. Biol. Chem.* **281**, 8469–8475 (2006).
- Pisareva, V. P. & Pisarev, A. V. eIF5 and eIF5B together stimulate 48S initiation complex formation during ribosomal scanning. *Nucleic Acids Res.* **42**, 12052–12069 (2014).
- Shah, P., Ding, Y., Niemczyk, M., Kudla, G. & Plotkin, J. B. Rate-limiting steps in yeast protein translation. *Cell* **153**, 1589–1601 (2013).
- Chu, D. et al. Translation elongation can control translation initiation on eukaryotic mRNAs. *EMBO J.* **33**, 21–34 (2014).
- Schuller, A. P., Wu, C. C. C., Dever, T. E., Buskirk, A. R. & Green, R. eIF5A functions globally in translation elongation and termination. *Mol. Cell* **66**, 194–205 (2017).
- Ingolia, N. T., Ghaemmghami, S., Newman, J. R. S. & Weissman, J. S. Genome-wide analysis *in vivo* of translation with nucleotide resolution using ribosome profiling. *Science* **324**, 218–223 (2009).
- Heyer, E. E. & Moore, M. J. Redefining the translational status of 80S monosomes. *Cell* **164**, 757–769 (2016).
- Ingolia, N. T. et al. Ribosome profiling reveals pervasive translation outside of annotated protein-coding genes. *Cell Rep.* **8**, 1365–1379 (2014).
- Juszkiewicz, S. et al. ZNF598 is a quality control sensor of collided ribosomes. *Mol. Cell* **72**, 469–481 (2018).
- Ikeuchi, K. et al. Collided ribosomes form a unique structural interface to induce Hel2-driven quality control pathways. *EMBO J.* **38**, e100276 (2019).

**Publisher's note** Springer Nature remains neutral with regard to jurisdictional claims in published maps and institutional affiliations.

© The Author(s), under exclusive licence to Springer Nature Limited 2019



## METHODS

No statistical methods were used to predetermine sample size. The experiments were not randomized. The investigators were not blinded to allocation during experiments and outcome assessment.

**The strategy for labelling with a ybbR tag.** The ybbR-tag labelling strategy has previously been established<sup>31</sup>. In brief, 4'-phosphopantetheinyl transferase (SFP synthase) specifically transfers a CoA conjugate to a serine residue in the ybbR tag (an 11-amino-acid peptide sequence), resulting in the covalent linking of the CoA conjugate to the ybbR tag. The SFP synthase that was used in this study was purified as previously described<sup>31</sup>, and the Cy3-like dye analogue CoA 547 was purchased from New England Biolabs (S9349). Following the published protocol, we synthesized CoA-Cy5.5 dye by reacting CoA trithium salt (Sigma-Aldrich, C3019-25MG; 0.52 mg, 0.66  $\mu$ mol, 0.75 equivalent (equiv.)) with sulfo-cyanine5.5 maleimide (Lumiprobe, 17380; 1 mg, 0.88  $\mu$ mol, 1 equiv.) at room temperature for 2 h in a 1-ml volume of 100 mM potassium phosphate pH 7.05 and 10% DMSO. This was followed by quenching the excess amount of maleimide with 8 mM DTT at room temperature for 10 min, which enables the product to be used without the need of further purification.

**Unlabelled and labelled tRNAs and yeast ribosomal subunits.** Native yeast Met-tRNA<sup>Met</sup> was purchased from tRNA Probes, LLC (MI-60) and *E. coli* Phe-tRNA<sup>Phe</sup> and Lys-tRNA<sup>Lys</sup> labelled with Cy3.5 or Cy5 were previously characterized<sup>32</sup>. Unlabelled yeast ribosomal subunits were purified by sucrose density-gradient centrifugation as previously described<sup>13</sup>. Cy3-40S was prepared by the ybbR-tag labelling method as described in the next two sections below.

**Genetically tagging the 40S subunit at uS19 with a ybbR tag.** The yeast uS19 (*RPS15*) strain JD1346 (*his3 $\Delta$ 1*; *leu2 $\Delta$ 0*; *ura3 $\Delta$ 0*; *YOL040c::KanMX4*; *pFL38(Pgal::RPS15; URA3)*) and plasmid pJD1055 (*pRP515-HIS3*) were provided by J. D. Dinman<sup>33</sup>. A ybbR-tag sequence (GATTCTCTGAATTTATTGCTAGTAGAAGCTTGCG)<sup>31</sup> was inserted at the N-terminal end of the uS19 sequence in the plasmid pJD1055, resulting in the plasmid pJFW1. This was introduced into yeast JD1346 using a standard lithium acetate yeast-transformation protocol<sup>34</sup> followed by a 5'-FOA plasmid shuffle<sup>35</sup>, to obtain the yeast strain yJFW11 in which all the 40S ribosomal subunits were tagged. For ybbR-uS19-40S purification, the yeast strain yJFW11 was streaked onto a selection plate containing synthetic complete-His (SC-His) medium. A single colony was used to inoculate 5 ml of fresh SC-His liquid medium, and the culture was grown at 30 °C overnight with shaking at 200 r.p.m. The next morning, the stationary-phase yeast culture was used to inoculate a 1.8-l culture of YPAD medium with a 1:4,000 dilution for large-scale growth until an optical density at 600 nm (OD<sub>600 nm</sub>) of around 0.6 was reached, before collecting cells by fast centrifugation at 4 °C and 7,808g in a Fibrelite F9-6x1000 LEX Fixed Angle Rotor (Thermo Fisher Scientific) for 12 min. The cell pellet was flash-frozen in liquid nitrogen before storage at -80 °C for further ribosome purification.

**Labelling of ybbR-uS19-40S.** For labelling of the 40S subunit through the ybbR tag, a 300- $\mu$ l labelling reaction was prepared by mixing 1  $\mu$ M 40S, 2  $\mu$ M SFP synthase and 10  $\mu$ M CoA-547 dye in a buffer containing 50 mM HEPES-KOH pH 7.5, 1 mM DTT and 10 mM MgCl<sub>2</sub>. The reaction was incubated at 30 °C for 30 min. To purify the labelled 40S from free dye, 150  $\mu$ l of the reaction mixture was loaded on top of a 750- $\mu$ l sucrose cushion (30 mM HEPES-KOH pH 7.5, 2 mM DTT, 100 mM KOAc, 5 mM Mg(OAc)<sub>2</sub> and 0.5 M sucrose) for ultracentrifugation at 351,955g at 4 °C for 90 min in a TLA100.2 rotor. The pellet containing labelled 40S was washed once with and then resuspended in the ribosome storage buffer (50 mM HEPES-KOH pH 7.5, 2 mM DTT, 100 mM KOAc, 3 mM Mg(OAc)<sub>2</sub>, 0.25 M sucrose) and stored at -80 °C after flash-freezing with liquid nitrogen.

**Labelling of 60S.** The Cy5-labelled SNAP-tagged 60S was prepared as previously described and characterized<sup>32</sup>. The Cy5.5-labelled ybbR-tagged 60S was prepared in the same way as described above for the Cy3-40S. For yeast genetics, the pRS315 plasmid used for the SNAP-tagged 60S yeast strain was mutated to carry the native uL18 (RPL5) gene sequence with a ybbR-tag sequence fused in frame at the C terminus before the stop codon. The new plasmid was transformed into JWY3733 strain (*MAT $\alpha$* ; *ura3-52*; *trp1 $\Delta$ 101*; *leu2 $\Delta$ 1*; *ade1*; *his3 $\Delta$ 200*; *rpl1::TRP1*+ pRS316-RPL5) and plated onto SC-Leu plates, followed by screening for the loss of the pRS316-RPL5 on SC-Leu plates containing 5'-FOA. The resulting strain (*MAT $\alpha$* ; *ura3-52*; *trp1 $\Delta$ 101*; *leu2 $\Delta$ 1*; *ade1*; *his3 $\Delta$ 200*; *rpl1::TRP1*+ pRS315-RPL5-ybbR) expresses uL18-ybbR as the sole source of the protein. The ybbR ribosome labelling efficiencies were generally around 75% based on absorbance measurements.

**Purification of protein factors.** Published strains, constructs and protocols were used for the purification of yeast eIF2, eIF3, eIF4E, eIF5, eIF5A, eIF5B (residues 396–1002), eEF1A, eEF1B $\alpha$ , eEF2 and eEF3<sup>13,15,32,36</sup>.

**Purification of eIF1.** The *SUI1* gene was cloned into a pET28 vector such that the overexpressed protein had the following sequence: MGSSHHHHHHM ENLYFQG-native eIF1, wherein the underlined sequence is a tobacco etch virus (TEV) protease cleavage site that cleaves between the Q and the G and this cleavage site is followed by the native eIF1 sequence. The final purified protein sequence is therefore the native eIF1 sequence, preceded by a Gly

residue. The plasmid was transformed into Rosetta2(DE3) *E. coli* cells. Protein overexpression was performed at an OD<sub>600 nm</sub> of around 0.6 by induction with 1 mM IPTG at 30 °C for 4 h. Cells were pelleted and stored at -80 °C. The pellet was rapidly thawed and suspended in 50 mM potassium phosphate (pH 7.5), 500 mM KCl, 10 mM imidazole, 5 mM  $\beta$ -mercaptoethanol ( $\beta$ ME), 10% (v/v) glycerol and 1 mM phenylmethylsulfonyl fluoride (PMSF). The cells were lysed by sonication and the lysate was clarified by centrifugation at 41,656g for 30 min at 4 °C in a F21-8x50y rotor (Thermo Fisher Scientific). The clarified lysate was loaded onto a 2-ml Ni-NTA column and washed with 50 ml wash buffer (50 mM potassium phosphate (pH 7.5), 300 mM KCl, 20 mM imidazole, 5 mM  $\beta$ ME, 10% (v/v) glycerol). Histidine (His)-tagged protein was eluted with wash buffer containing 250 mM imidazole. The eluted protein was diluted five times in volume by addition of 20 mM HEPES-KOH pH 7.5, 10% (v/v) glycerol and 2 mM DTT, and loaded to a 5-ml HiTrap Heparin HP column for further purification as previously described<sup>13</sup>. The eluate was treated with TEV protease overnight on ice to cleave off the 6 $\times$ His tag and eIF1 was recovered by flowing through a Ni-column to remove the free tag and TEV protease. The final eIF1 protein was purified on a HiLoad 26/600 Superdex 200-pg gel filtration column in storage buffer (20 mM HEPES-KOH pH 7.5, 100 mM KOAc, 10% (v/v) glycerol, 2 mM DTT), flash-frozen with liquid nitrogen and stored at -80 °C.

**eIF1A.** The *TIF11* gene was cloned into a pET28 vector such that the overexpressed protein had the following sequence: MGSSHHHHHHH MENLYFQG-native eIF1A, and the final purified protein sequence is the native eIF1A sequence preceded by a Gly residue. The protein overexpression and purification were performed in exactly the same way as for eIF1.

**eIF4A.** The *TIF1* gene was cloned into a pET28 vector such that the overexpressed protein had the following sequence: MGSSHHHHHHH MENLYFQG-native eIF4A, and the final purified protein sequence is the native eIF4A sequence preceded by a Gly residue. The protein overexpression and Ni-NTA purification were performed in the same way as for eIF1. After Ni-NTA purification, the protein was treated with TEV protease overnight to cleave off the 6 $\times$ His tag, while dialysing at 4 °C against a buffer containing 50 mM potassium phosphate (pH 7.5), 300 mM NaCl and 5 mM  $\beta$ ME. The eIF4A protein was recovered by flowing through a Ni-column to remove the cleaved 6 $\times$ His tag and TEV protease. The final protein was purified on a HiLoad 26/600 Superdex 200-pg gel filtration column in storage buffer (20 mM HEPES-KOH pH 7.5, 100 mM KOAc, 2 mM DTT), flash-frozen with liquid nitrogen and stored at -80 °C.

**eIF4B.** The *TIF3* gene was cloned into a pET22b vector such that the overexpressed protein had the following sequence: native eIF4B-ENLYFQGAAAELHHHHHHH, and the final purified protein sequence is the native eIF4B sequence followed by ENLYFQ. The protein overexpression and purification were performed in exactly the same way as for eIF4A.

**eIF4G.** The *TIF4631* gene was cloned into the multiple-cloning site 1 of a pET-Duet-1 vector such that the overexpressed protein had the following sequence: native eIF4G-ENLYFQGHHHHHH, and the final purified protein sequence is the native eIF4G sequence followed by ENLYFQ. On the same plasmid, the native eIF4E gene (*CDC33*) was cloned into the multiple-cloning site 2, which has been proven to facilitate the overexpression of the full-length eIF4E in *E. coli*<sup>37</sup>. The protein overexpression and purification were performed in the same way as for eIF4A, except that 500 mM KCl was included in all the buffers used for the Ni-column purification. The final protein contained both eIF4G and wild-type eIF4E and the full-length eIF4G migrates slower than expected on SDS-PAGE for its molecular weight, which has previously been shown<sup>37–39</sup>. The full-length nature of eIF4G was further verified by Edman degradation and mass spectrometry.

**eIF5B variants.** When applicable, a ybbR-tag sequence was introduced into the pMGHisTev5B plasmid<sup>13</sup> after the TEV cleavage site, with or without a T439A or H505Y mutation, by site-directed mutagenesis. The protein was overexpressed and purified following the previously described protocol<sup>13</sup>. For full-length eIF5B, we started with the plasmid pC1005<sup>40</sup>, deleted the Flag-tag sequence, inserted in a 8 $\times$ His tag and a TEV cleavage site before the native eIF5B sequence, and cloned into the multiple-cloning site 1 of the pETDuet-1 vector. Proteins were overexpressed in Rosetta2(DE3) cells as described for eIF1 and the purification was performed as previously described<sup>13</sup>. To label the ybbR-tagged proteins with Cy5.5, 10  $\mu$ M protein was incubated with 2  $\mu$ M SFP synthase and 15  $\mu$ M CoA-Cy5.5 dye in a buffer containing 50 mM HEPES-KOH pH 7.5, 1 mM DTT and 10 mM MgCl<sub>2</sub> at room temperature for 30 min. The reaction mixture was loaded onto a Ni-NTA column equilibrated with the same buffer to remove His-tagged SFP synthase, and the flow-through was passed through a 10-DG desalting column to remove free dye from the protein. The final protein was purified on a Superdex 75 10/300 GL column in storage buffer (20 mM HEPES-KOH pH 7.5, 100 mM KOAc, 10% glycerol, 2 mM DTT) and stored at -80 °C. The ribosome-dependent GTPase activity was determined as previously described using the malachite green assay<sup>32</sup>.

**mRNAs.** All the mRNAs were prepared by T7 RNA polymerase run-off transcription. The RNA transcript sequences are as follows (with the start and stop codons underlined): model mRNA: GG(UC)<sub>8</sub>UAUGUUCAAUAA(UC)<sub>16</sub>; model mRNA-Kozak: GG(UC)<sub>8</sub>UAAAAAAAAUGUUCAAUAA(UC)<sub>16</sub>; model mRNA-Kozak<sub>-3U</sub>: GG(UC)<sub>8</sub>UAAAAAUGUUCAAUAA(UC)<sub>16</sub>; *RPL1A1*: GGAGAC CACAUCGAUCAAUCGAAUGUUCGCCAAGUGGAGAAAGAAGAGAA CUAGAAGACUAAAGAGAAAGAGACGGAAAGGUGAGAGCCAGAUCCAAA UAA; *RPL30*: GGAACACAGACCGGAGUGUUUAGAACCUCAGCUAAUU CAAUUAUCAAUUACGCAGAGUGUUCCAGUUAAUCCCAAGAUC UAUCAACCAAAGUUGGCUUUGGUUAUCAGUCUGGUAAGUACACCU UAGGUACAAGUCCACUGUCAAGUCUUUGAGACUAAAGGUAAGUCUAA GUUGAUCUAUUGGCCGUAACACUCCAGUUUUUGAGAAAGUCCGAU UGGAUAUUACGCUAUGUUGUCCAAGACUAAGGUCUACUACUCCAA GGUGGUAACAACGAAUUGGUACUGCUGUCGGUAAGUUUAUCAGAG UCGGUGUUGUCUCUAUUUUGGAAGCUGGUGACUCUGAUUCUUGAC CACCUUGGCUAAUAAGGUAAGUCAAACGAAUUU.

For the model mRNA, model mRNA-Kozak and model mRNA-Kozak<sub>-3U</sub>, 3'-end biotinylation or Cy5-labelling was performed using periodate chemistry followed by hydrazide reaction as previously described<sup>41</sup>. The RNA was purified from the free hydrazide on a Superdex 75 10/300 GL column in storage buffer (20 mM HEPES-KOH pH 7.5 and 100 mM KOAc) and stored at -80 °C. The hydrazide analogues used were EZ-Link Biotin-LC-Hydrazide (Thermo Fisher Scientific, 21340) and cyanine5 hydrazide (Lumiprobe, 13070).

To obtain 3'-end-biotinylated or Cy3-labelled, fully m<sup>7</sup>G-capped *RPL1A1* mRNA, the RNA transcript was: (1) ligated to a DNA oligonucleotide (5'pd(CT)<sub>12</sub>-biotin-3' or 5'pd(CT)<sub>6</sub>-Cy3-d(CT)<sub>6</sub>-3') (TriLink Biotechnologies) and gel purified; (2) m<sup>7</sup>G-capped using the Vaccinia capping system (New England BioLabs, M2080S); and (3) treated with RNA 5' polyphosphatase (Epicentre, RP8092H) and terminator 5'-phosphate-dependent exonuclease (Epicentre, TER51020) to remove uncapped RNA, followed by phenol and chloroform extraction and ethanol precipitation.

The 3'-end-biotinylated, fully m<sup>7</sup>G-capped *RPL30* mRNA was prepared by: (1) 3'-end biotinylation using the periodate chemistry and hydrazide reaction<sup>41</sup>; and (2) m<sup>7</sup>G-capping and uncapped-RNA depleting as described above for *RPL1A1* mRNA. **Native gel-shift analyses.** The formation of pre-initiation and initiation complexes was monitored by 4% native PAGE analyses using protocols as previously described<sup>13</sup>. Samples were prepared in 1 × Recon buffer (30 mM HEPES-KOH pH 7.5, 100 mM KOAc, 3 mM Mg(OAc)<sub>2</sub>). A ternary complex was prepared by incubating 3.9 μM eIF2 with 1 mM GTP:Mg<sup>2+</sup> at 30 °C for 10 min, followed by addition of 2.7 μM Met-tRNA<sup>Met</sup>; and incubation at 30 °C for another 5 min.

For reactions with the model mRNA (Extended Data Fig. 2a), the 48S PIC was formed by mixing a final concentration of 1 μM eIF1, 1 μM eIF1A, three-fold-diluted ternary complex (final 1.3 μM eIF2 and 0.9 μM Met-tRNA<sup>Met</sup>), 50 nM Cy3-40S and 2 μM model mRNA-Cy5, and incubating at 30 °C for 15 min; the 80S PIC was formed by addition of a final concentration of 1 μM eIF5, 1 μM eIF5B and 200 nM 60S to the 48S PIC and further incubation at 30 °C for 5 min. Typically, 10 μl of each sample was mixed with 2 μl of native gel dye (50% sucrose, 0.02% bromophenol blue in 1 × Recon buffer) and loaded into the 4% native PAGE gel for electrophoresis<sup>13</sup>; this was followed by scanning the gel for the Cy3 and Cy5 fluorescence with a Typhoon scanner.

For reactions with the cap-*RPL1A1* mRNA (Extended Data Fig. 2b), the samples were prepared similarly to above, except 1 mM ATP:Mg<sup>2+</sup> was supplemented into the reaction buffer, the cap-*RPL1A1*-Cy3 mRNA was at 100 nM, 40S was unlabelled and, when applicable, 1 μM eIF4A, 1 μM eIF4B, 400 nM eIF4G, 200 nM eIF4E and 200 nM eIF3 were added.

**Single-molecule inter-subunit FRET experiments using a total internal reflection fluorescence microscope.** The ribosomal inter-subunit FRET signal was characterized on a previously described<sup>42,43</sup> home-built, prism-based total internal reflection fluorescence microscope. The 80S complexes were assembled using Cy3-40S and Cy5-60S on the model mRNA-biotin in the same way as for the native gel shift assays. The 80S complexes were immobilized on a neutravidin-derivatized quartz slide according to reported protocols<sup>32,43</sup>. Unbound components were washed from the slide with 1 × Recon buffer supplemented with 1 mM GTP:Mg<sup>2+</sup> and an oxygen-scavenging system (containing 2.5 mM PCA (protocatechuic acid), 2.5 mM TSY and 2 × PCD (protocatechuate-3,4-dioxygenase), purchased from Pacific Bioscience). Cy3 fluorophores were excited with a diode-pumped solid-state 532-nm laser at 1 kW cm<sup>-2</sup>. Fluorescence intensity trajectories were recorded at 10 frames per second with a total of 600 frames collected per movie by using the MetaMorph imaging software (Molecular Devices). Analysis of fluorescence intensity trajectories was performed in MATLAB using custom scripts<sup>42</sup>. Baseline correction of raw fluorescence traces and Cy3 signal bleed-through into the Cy5 channel were corrected on a trace-by-trace basis. The FRET states were assigned with a hidden Markov model-based approach as previously described and visually corrected<sup>42</sup>.

**Real-time single-molecule experiments on the ZMW instrument.** All the experiments were performed in the 1 × Recon buffer supplemented with 1 mM GTP:Mg<sup>2+</sup> (and 1 mM ATP:Mg<sup>2+</sup> for m<sup>7</sup>G-capped mRNAs) unless otherwise specified. A ZMW-based PacBio RSII instrumentation<sup>14</sup> was used for all the real-time measurements at 20 °C, 26 °C or 30 °C. For experiments performed with the model mRNA, model mRNA-Kozak and model mRNA-Kozak<sub>-3U</sub>, in general, immediately before each experiment, the 48S PIC was formed as described for the native gel shift assays using final concentrations of 80 nM Cy3-40S, 500 nM biotinylated mRNA, 1 μM eIF1, 1 μM eIF1A, 300 nM eIF5, 1.3 μM eIF2 and 0.9 μM Met-tRNA<sup>Met</sup>. In parallel, a ZMW chip was treated with 0.2% (w/v) Tween20 at room temperature for 10 min followed by treatment with neutravidin at room temperature for 5 min, which bound to the biotin-PEG (polyethylene glycol) on the chip. After immobilizing the 48S PIC via the biotin on the mRNA onto the neutravidin-coated surface, the chip was washed twice using an imaging buffer containing the oxygen-scavenging system and 62.5 μg ml<sup>-1</sup> casein to remove unbound complexes, and loaded onto the RSII instrument in the presence of 20 μl of the imaging buffer. At the same time, a delivery mixture containing 200 nM Cy5-60S, 1 μM eIF5, eIF5B (2 μM unlabelled or 40 nM Cy5.5-labelled), Cy3.5-Phe-TC (pre-formed by incubating 8 μM eEF1A, 10 μM eEF1Bα with 1 mM GTP:Mg<sup>2+</sup> at room temperature for 5 min, followed by the addition of 0.8 μM Cy3.5-Phe-tRNA<sup>Phe</sup> and another incubation at room temperature for 5 min; diluted eightfold in the delivery mixture for final 50 nM ternary complex or fourfold for final 100 nM ternary complex), oxygen-scavenging system and 62.5 μg ml<sup>-1</sup> casein was prepared and loaded onto the instrument. For each experiment, the instrument delivered 20 μl of the delivery mixture to the chip at the beginning of the experiment, and recorded a 15-min movie at 10 frames per second, with 0.32 μW μm<sup>-2</sup> of 532-nm laser illumination (for unlabelled eIF5B experiments), or 0.6 μW μm<sup>-2</sup> of 532-nm laser and 0.1 μW μm<sup>-2</sup> of 642-nm laser dual illumination (for Cy5.5-labelled eIF5B experiments). For the elongation assay with tRNA-tRNA smFRET, both the imaging buffer and the delivery mixture were supplemented with 1 mM ATP, and the delivery mixture contained 115 nM Cy5.5-60S, 1 μM eIF5, 2 μM eIF5A, 2 μM eIF5B, 1 μM eEF2, 400 nM eEF3, 100 nM Cy3.5-Phe-TC and 100 nM Cy5-Lys-TC (pre-formed separately by incubating 8 μM eEF1A, 10 μM eEF1Bα with 1 mM GTP:Mg<sup>2+</sup> at room temperature for 5 min, followed by the addition of 0.8 μM Cy3.5-Phe-tRNA<sup>Phe</sup> or Cy5-Lys-tRNA<sup>Lys</sup> and another incubation at room temperature for 5 min), oxygen-scavenging system and 62.5 μg ml<sup>-1</sup> casein. The imaging was performed at 20 °C with 0.32 μW μm<sup>-2</sup> of 532-nm laser illumination.

Experiments with the cap-*RPL1A1* and cap-*RPL30* mRNAs were performed in a similar manner, except that 1 μM eIF4A, 1 μM eIF4B, 0.67 μM eIF4E, 300 nM eIF4G and 200 nM eIF3 were also included in the second incubation step for the 48S PIC formation, and 300 nM eIF3 was also added to the delivery mixture. When titrating free Mg<sup>2+</sup> concentrations, the corresponding amount of Mg(OAc)<sub>2</sub> was used in both the imaging buffer and the delivery mixture. When additional protein factors were added to each experiment, they were added to the delivery mixture in the denoted amounts. For experiments performed with GDPNP, the 48S PIC was formed in the presence of GTP as described above. After immobilization, the imaging buffer used contained 0.2 mM GTP; no GTP was added in the delivery mixture and 6 mM GDPNP:Mg<sup>2+</sup> was added instead.

The resulting experimental movies were analysed using custom MATLAB scripts, as previously described<sup>14</sup>. In brief, fluorescence traces from the ZMWs were filtered on the basis of the presence of the fluorophores of interests at different time points (the signal from immobilized 48S PICs was expected to be present at the beginning of the movie, whereas signals from fluorophores attached to the 60S, eIF5B and tRNA were expected not to be). The different arrival and departure events were manually assigned based on the appearance and disappearance of the corresponding fluorescent signals.

**Cryo-EM analysis of the 48S PIC formed with cap-*RPL30* mRNA.** The 48S PIC sample for the cryo-EM analysis was prepared in the same way as that for the real-time single-molecule experiments in the presence of ATP, GTP and 3 mM free Mg<sup>2+</sup>. After the incubation at 30 °C, 30 μl of the sample was diluted with 100 μl 1 × Recon buffer and then concentrated to 30 μl using a Vivaspin 500 concentrator (100,000 MWCO PES, Sartorius, VS0141) by centrifugation at 6,973g for 5 min at 4 °C. This step mimics the washing step in our single-molecule experiments for removing unbound components. A 3 μl sample was applied to each 25-s glow-discharged (in a PELCO easiGlow glow discharger, Ted Pella, Inc.) 200-mesh Quantifoil R2/1 gold grid (Electron Microscopy Sciences, Q250AR1) at 21 °C and 95% humidity. The grid was blotted for 2 s before plunging into liquid ethane using a Leica EM GP (Leica Microsystems). Automated data acquisition was performed using SerialEM<sup>44</sup> on a Tecnai F20 microscope operated at 200 kV at a dose rate of 10 e<sup>-</sup> per pixel per s using a defocus range of -2.0 to -4.0 μm. Eighty movie-mode images with 10-s exposure time and 50 frames for each were recorded on a Gatan K2 Summit direct electron detector camera in a counting mode at a nominal magnification of 14,500 (yielding a pixel size of 2.53 Å on the specimen level). The drift correction was performed using MotionCor2<sup>45</sup> and the contrast transfer



function (CTF) estimation was performed using CTFFIND-4.1<sup>46</sup>. The images with bad CTF fitting were excluded and 78 images were selected for further data processing. The initial particle-picking was performed using EMAN2<sup>47</sup> and the saved box files were imported into RELION-3.0-beta-2<sup>48</sup> for the first 2D classification to generate some good 2D class averages as a new template for automatic particle-picking in RELION. The 3D initial model was built using RELION. After the first six-class 3D classification, 11,478 particles within one class from a total of 17,654 good particles were selected for the 3D auto-refine to obtain a map at 9.0-Å resolution (not shown). Then a soft mask around the Met-tRNA<sup>Met</sup><sub>i</sub> region was created to perform the particle subtraction followed by the focused classification (without image alignment) into two classes: with Met-tRNA<sup>Met</sup><sub>i</sub> and without Met-tRNA<sup>Met</sup><sub>i</sub>. Finally, 4,930 particles were selected for the final 3D auto-refine to reconstruct the map at 9.9-Å resolution. The scanning-competent open (EMD 3049) or scanning-incompetent closed (EMD 3048) 48S PIC structures were low-pass-filtered to the same resolution (9.9 Å) and scaled to the same pixel size using the command `relion_image_handler` in RELION for visual comparisons in Chimera (UCSF) (see Extended Data Fig. 2c–e).

**Cryo-EM analysis of the on-pathway 80S complexes during initiation and the transition to elongation.** To probe the conformational states of the 80S complexes along the native initiation and transition to elongation pathways, we decided to analyse the sample corresponding to the reaction time point 45 s (under pre-steady-state conditions), when the 80S initiation complex should account for around 64.5% (and the 80S elongation complex account for around 35.5%; see Supplementary Note) of the total 80S complexes assembled on the model mRNA at 20 °C and 3 mM Mg<sup>2+</sup> in the presence of wild-type eIF5B and GTP. Also, to ease the post-acquisition particle-classification procedure, we decided to use excess 48S PICs to 60S, such that free 60S particles would be minimized. To this end, we assembled 48S PICs in the same way as in the single-molecule experiments with the model mRNA at 3 mM free Mg<sup>2+</sup>, and the only difference was that the concentration of the unlabelled 40S was 300 nM (assuming 100% complex assembly, the 48S PIC concentration should be 300 nM). In parallel, an initiation mixture containing 150 nM unlabelled 60S, 1 μM eIF5 and 2 μM eIF5B was prepared. After mixing equal volumes of the 48S PIC with the initiation mixture, the final concentrations were 150 nM 48S PIC, 75 nM 60S and 1 μM eIF5B. At 20 °C under these conditions, we would expect the reaction kinetics to be similar to that of the single-molecule experiments described above.

While the 48S PIC and initiation mixtures were kept on ice, the 200-mesh R2/1 Quantifoil grids were glow-discharged for 25 s. When the Leica EM GP system was ready for grid plunging, 5 μl of the 48S PIC mixture was mixed with 5 μl of the initiation mixture, and incubated at about 20 °C for 30 s before approximately 3 μl of the sample was applied to each grid. The grid was immediately blotted for 2 s using a filter paper before being plunged into liquid ethane with 95% chamber humidity at about 21 °C (resulting in a reaction time from mixing to grid-freezing at 45 s). Automated data acquisition was done using SerialEM<sup>44</sup> on a Tecnai F20 microscope operated at 200 kV at a dose rate of 10 e<sup>-</sup> per pixel per s using a defocus range of -0.7 to -2.5 μm. A total of 226 movie-mode images with 10-s exposure time and 50 frames for each were recorded on a Gatan K2 Summit direct electron detector camera in a counting mode at a nominal magnification of 14,500 (yielding a pixel size of 2.53 Å on the specimen level). The drift correction was performed using MotionCor2<sup>45</sup> and the CTF estimation was done using CTFFIND-4.1<sup>46</sup>. The images with bad CTF fitting, too much drift or that were over-focused were excluded, and eventually 134 images were selected for further 2D and 3D classifications. The initial particle-picking was performed using EMAN2<sup>47</sup> and the saved box files were imported into RELION-3.0-beta-2<sup>48</sup> for the first 2D classification, to generate some good 2D class averages as a new template for better 80S particle-picking in RELION. The 3D initial model of the 80S complex was built using RELION. The following 2D and 3D classifications were used to eliminate junk or bad particles, or even free 40S or 60S particles. In total, 25,144 80S particles were selected for the 3D auto-refine to obtain the map at 7.8-Å resolution (not shown). The eIF5B Protein Data Bank (PDB) model was selected from the PDB file 4V8Z<sup>12</sup> and fitted into the 7.8-Å 80S map. A zone with radius 6 around the fitted eIF5B PDB model was generated using Chimera. Then a soft mask around the eIF5B density was made using mask creation in RELION. The particle subtraction was done with this soft mask to perform the focused 3D classification (without image alignment) into two classes of 80S: 17,602 particles with eIF5B bound (class 1, 80S initiation complex; Extended Data Fig. 10c) and 7,542 without eIF5B (class 2, 80S elongation complex; Extended Data Fig. 10d). Finally 3D auto-refine reconstructed the 80S initiation complex map at 8.4-Å resolution and the 80S elongation complex map at 10.1-Å resolution.

**Reporting summary.** Further information on research design is available in the Nature Research Reporting Summary linked to this paper.

## Data availability

Source data for figures are available as accompanying Source Data files. The cryo-EM maps have been deposited in the Electron Microscopy Data Bank

(EMDB) server under the accession codes EMD-20324 (48S PIC), EMD-20325 (80S initiation complex) and EMD-20326 (80S elongation complex). Single-molecule fluorescence-trace data are available upon request.

## Code availability

The MATLAB scripts used in this study are available at: <https://drive.google.com/drive/u/1/folders/1-yKC0Nui7T7yoJScCuODPhCT4G52emLj>

- Yin, J., Lin, A. J., Golan, D. E. & Walsh, C. T. Site-specific protein labeling by Sfp phosphopantetheinyl transferase. *Nat. Protoc.* **1**, 280–285 (2006).
- Petrov, A., Grosely, R., Chen, J., O'Leary, S. E. & Puglisi, J. D. Multiple parallel pathways of translation initiation on the CrPV IRES. *Mol. Cell* **62**, 92–103 (2016).
- Bowen, A. M. et al. Ribosomal protein uS19 mutants reveal its role in coordinating ribosome structure and function. *Translation* **3**, e1117703 (2015).
- Ito, H., Fukuda, Y., Murata, K. & Kimura, A. Transformation of intact yeast cells treated with alkali cations. *J. Bacteriol.* **153**, 163–168 (1983).
- Maniatis, T., Fritsch, E. F. & Sambrook, J. *Molecular Cloning: a Laboratory Manual* (Cold Spring Harbor Laboratory Press, 1982).
- O'Leary, S. E., Petrov, A., Chen, J. & Puglisi, J. D. Dynamic recognition of the mRNA cap by *Saccharomyces cerevisiae* eIF4E. *Structure* **21**, 2197–2207 (2013).
- Mitchell, S. F. et al. The 5'-7-methylguanosine cap on eukaryotic mRNAs serves both to stimulate canonical translation initiation and to block an alternative pathway. *Mol. Cell* **39**, 950–962 (2010).
- Algire, M. A. et al. Development and characterization of a reconstituted yeast translation initiation system. *RNA* **8**, 382–397 (2002).
- Goyer, C. et al. TIF4631 and TIF4632: two yeast genes encoding the high-molecular-weight subunits of the cap-binding protein complex (eukaryotic initiation factor 4F) contain an RNA recognition motif-like sequence and carry out an essential function. *Mol. Cell. Biol.* **13**, 4860–4874 (1993).
- Choi, S. K. et al. Physical and functional interaction between the eukaryotic orthologs of prokaryotic translation initiation factors IF1 and IF2. *Mol. Cell. Biol.* **20**, 7183–7191 (2000).
- Rinaldi, A. J., Suddala, K. C. & Walter, N. G. Native purification and labeling of RNA for single molecule fluorescence studies. *Methods Mol. Biol.* **1240**, 63–95 (2015).
- Marshall, R. A., Dorywalska, M. & Puglisi, J. D. Irreversible chemical steps control intersubunit dynamics during translation. *Proc. Natl Acad. Sci. USA* **105**, 15364–15369 (2008).
- Blanchard, S. C., Kim, H. D., Gonzalez, R. L. Jr, Puglisi, J. D. & Chu, S. tRNA dynamics on the ribosome during translation. *Proc. Natl Acad. Sci. USA* **101**, 12893–12898 (2004).
- Mastrorade, D. N. Automated electron microscope tomography using robust prediction of specimen movements. *J. Struct. Biol.* **152**, 36–51 (2005).
- Zheng, S. Q. et al. MotionCor2: anisotropic correction of beam-induced motion for improved cryo-electron microscopy. *Nat. Methods* **14**, 331–332 (2017).
- Rohou, A. & Grigorieff, N. CTFFIND4: fast and accurate defocus estimation from electron micrographs. *J. Struct. Biol.* **192**, 216–221 (2015).
- Tang, G. et al. EMAN2: an extensible image processing suite for electron microscopy. *J. Struct. Biol.* **157**, 38–46 (2007).
- Scheres, S. H. W. RELION: implementation of a Bayesian approach to cryo-EM structure determination. *J. Struct. Biol.* **180**, 519–530 (2012).
- Shin, B. S. et al. Structural integrity of α-helix H12 in translation initiation factor eIF5B is critical for 80S complex stability. *RNA* **17**, 687–696 (2011).
- Munro, J. B., Sanbonmatsu, K. Y., Spahn, C. M. T. & Blanchard, S. C. Navigating the ribosome's metastable energy landscape. *Trends Biochem. Sci.* **34**, 390–400 (2009).

**Acknowledgements** We are grateful to J. Lorsch, T. Dever, J. Dinman, J. Yin and C. Aitken for sharing constructs, strains and protocols; C. Sitron and O. Brandman for sharing equipment and knowledge for use of their Freezer/Mill cryogenic mill for yeast lysis; the Stanford PAN facility for mass spectrometry analyses of proteins; and members of the Puglisi laboratory for discussion and input. This work was supported by the US National Institutes of Health (NIH) grants GM113078 and AI047365 to J.D.P.; a Knut and Alice Wallenberg Foundation postdoctoral scholarship (KAW 2015.0406) to J.W.; a National Science Foundation Graduate Research Fellowship (DGE-114747) to A.G.J.; a Damon Runyon Fellowship funded by the Damon Runyon Cancer Research Foundation (DRG-2321-18) to C.P.L.; a Stanford Bio-X fellowship to J.C.; and a Stanford Interdisciplinary Graduate Fellowship and NIH Molecular Biophysics Training Grant T32-GM008294 to A.P.

**Author contributions** J.W. performed all the biochemical and single-molecule experiments; J.W. analysed the data with help from J.C., A.P. and A.N.P.; J.W. prepared the samples, D.-H.C. and J.W. acquired and D.-H.C. processed the cryo-EM data; J.W. and J.D.P. conceived the project with input from A.G.J., C.P.L. and A.N.P.; and J.W., A.G.J., C.P.L., J.C., D.-H.C. and J.D.P. wrote the manuscript.

**Competing interests** The authors declare no competing interests.

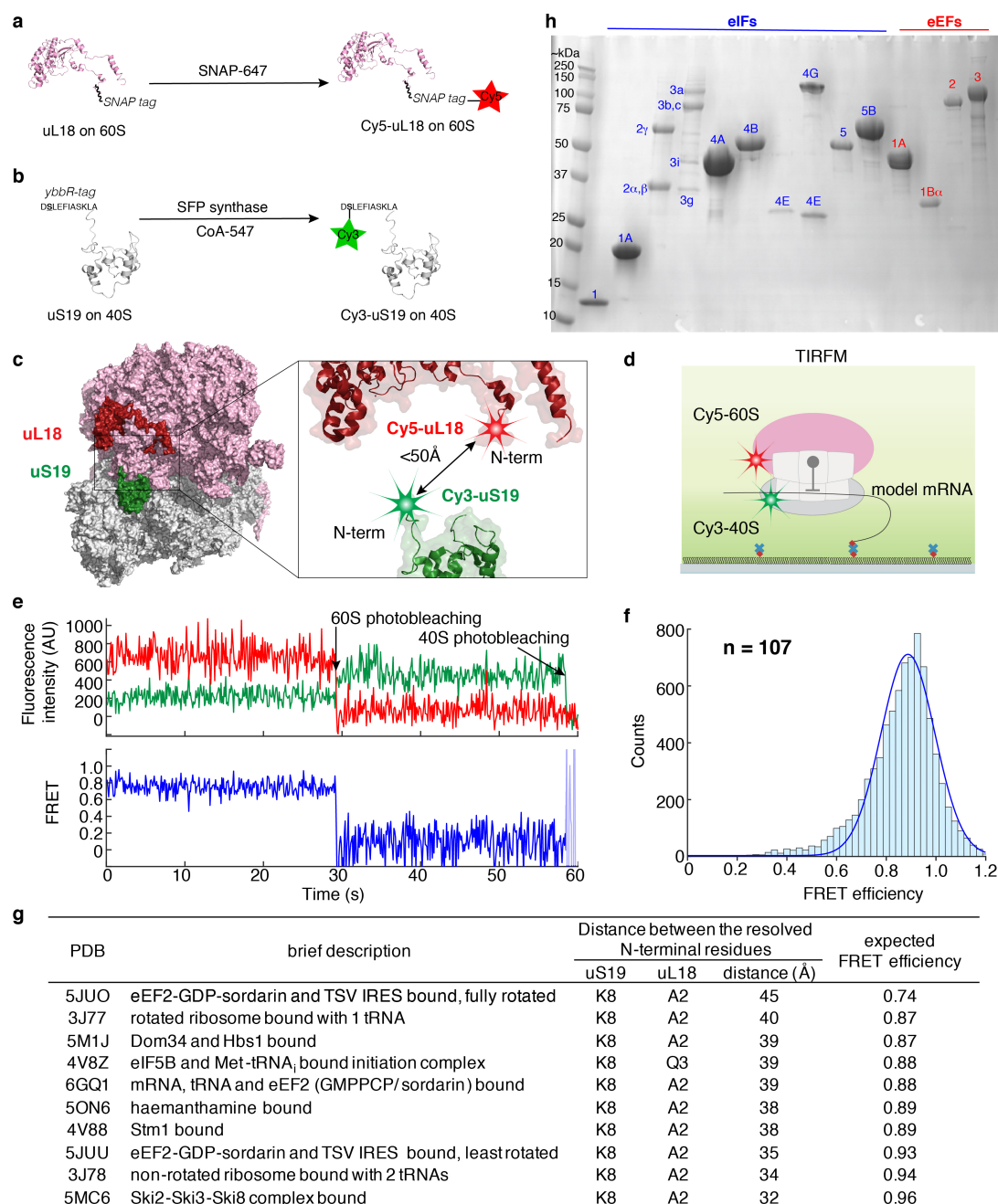
## Additional information

**Supplementary information** is available for this paper at <https://doi.org/10.1038/s41586-019-1561-0>.

**Correspondence and requests for materials** should be addressed to J.D.P.

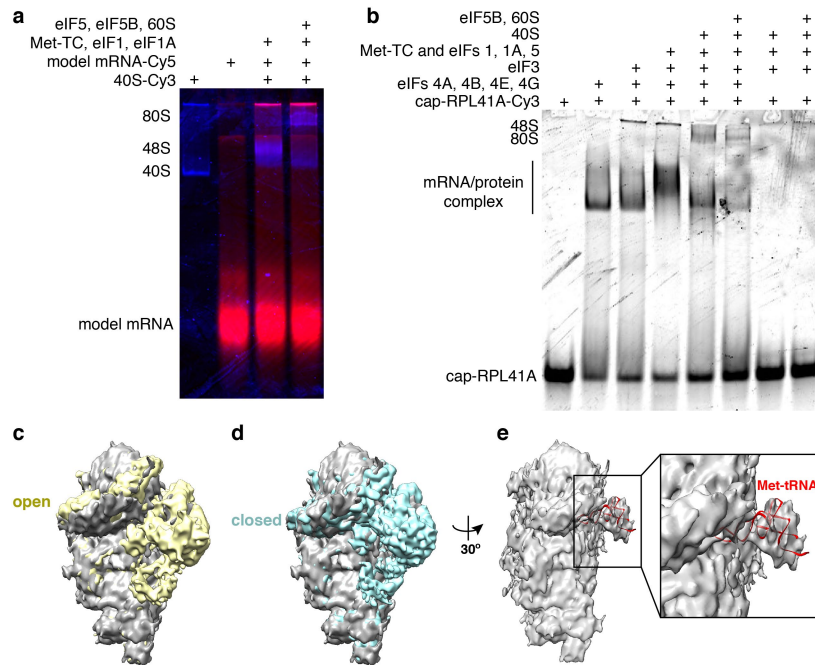
**Reprints and permissions information** is available at <http://www.nature.com/reprints>.





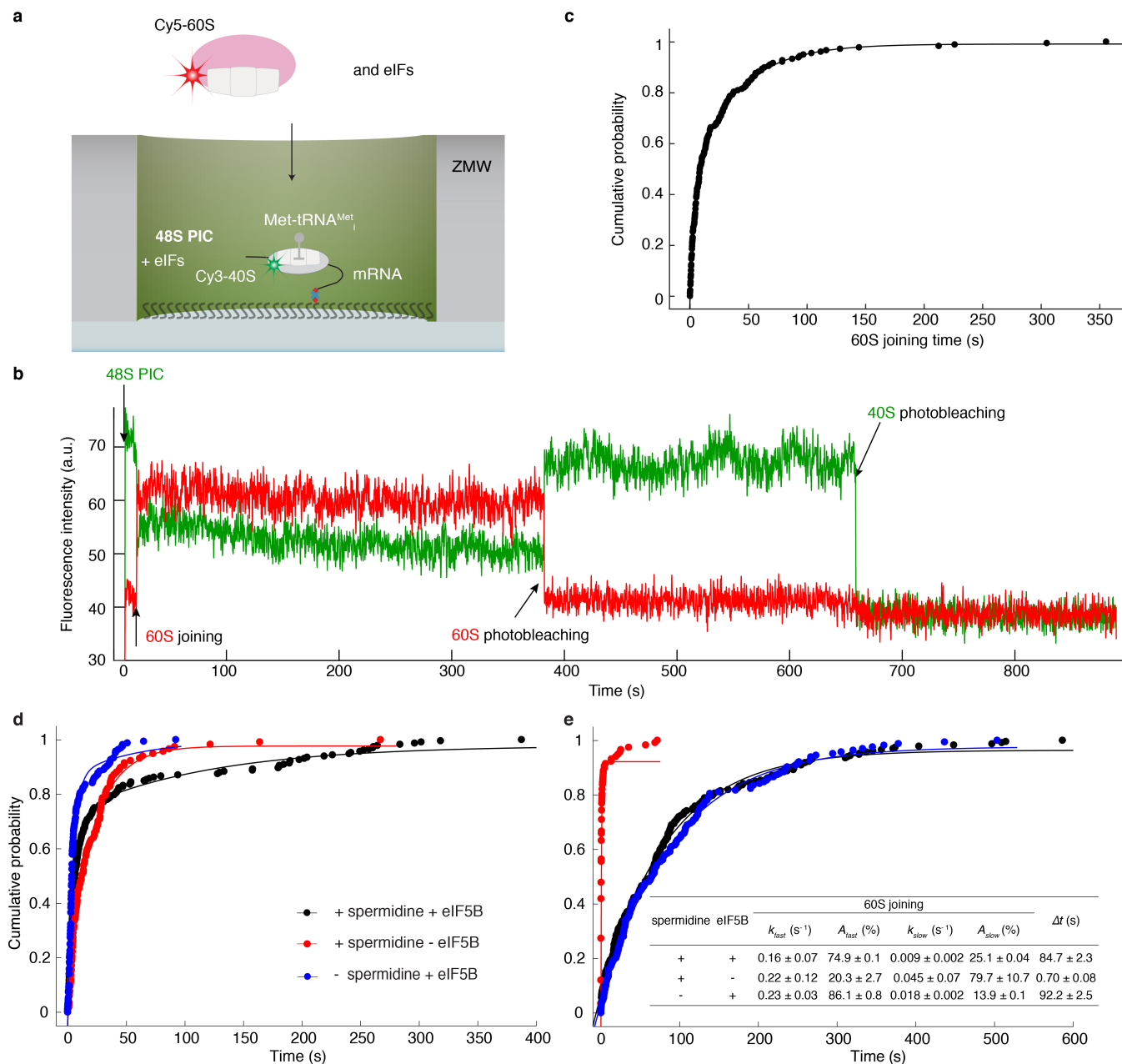
**Extended Data Fig. 1 | A reconstituted yeast translation system with fluorescently labelled ribosomes for inter-subunit smFRET.** **a**, The labelling of the yeast 60S ribosomal subunit with Cy5 by means of a SNAP tag fused to the uL18 protein and the reaction with a SNAP-647 dye have previously been established<sup>32</sup>. **b**, In this work, we engineered a yeast strain in which all of the 40S subunits carried the N-terminal ybbR-tagged uS19 protein. After purification, the 40S was labelled by SFP synthase with CoA-547 at the serine residue (in bold and underlined) of the ybbR tag, resulting in the Cy3-40S. **c**, The estimated distance between the 2 ribosomal labelling sites is within 50 Å of that from published yeast 80S 3D structures (**g**). The ribosome model was created in PyMOL, using data from PDB 4V8Z<sup>12</sup>. **d**, Total internal reflection fluorescence microscopy (TIRFM) experimental setup to characterize the inter-subunit FRET signal. 80S complexes were assembled from Cy3-40S and Cy5-60S on the

model mRNA (Fig. 1a) in the presence of the required factors (Methods), and were immobilized on a quartz slide used for TIRFM imaging with green laser illumination. **e**, **f**, Sample TIRFM experimental trace (**e**) and the inter-subunit smFRET efficiency histogram (**f**; fitted with a single-Gaussian distribution, with a mean FRET efficiency of  $0.89 \pm 0.15$  s.e.m.);  $n = 107$  molecules. **g**, Estimated distances between the two labelling sites on the ribosomal subunits from a few examples of published yeast 80S structures in different functional states, and the expected FRET efficiencies based on a Förster radius ( $R_0$ ) of 54 Å for the Cy3-Cy5 FRET pair. **h**, Representative SDS-PAGE analysis of the purified core eukaryotic initiation factors (blue numbering) and elongation factors (red numbering) that were used for the reconstitution of the translation system. Each component was analysed at least three times with similar results.



**Extended Data Fig. 2 | Native gel shift assays and cryo-EM analysis showing active translation initiation with our purified yeast translation system.** **a**, Representative gel showing initiation on the model mRNA. A merged view of Cy5 (red) and Cy3 (blue) scans of the same gel is shown. For gel source data, see Supplementary Fig. 1. The model mRNA was labelled with Cy5 and 40S was labelled with Cy3. Addition of Cy3–40S, Met-tRNA<sup>Met<sub>i</sub></sup>;eIF2:GTP (Met-TC), eIF1 and eIF1A to the model mRNA–Cy5 resulted in the formation of a distinct 48S PIC band. Further addition of eIF5, eIF5B and 60S led to the formation of the 80S band. The experiment was repeated three times with similar results. **b**, Representative gel showing initiation on the cap-*RPL41A* mRNA. For gel source data, see Supplementary Fig. 1. The cap-*RPL41A* mRNA was labelled with Cy3, and other components were unlabelled. The gel was scanned for Cy3 fluorescence. Various mRNA and protein complexes were formed in the absence of 40S. After adding 40S to the mixture, a distinct 48S PIC band was formed and further addition of eIF5B and 60S shifted this band to the 80S band. The apparent electrophoretic mobility of the 48S PIC that formed with the cap-*RPL41A* mRNA differs from that of the 48S PIC that formed with the model mRNA; this is probably a result of the different

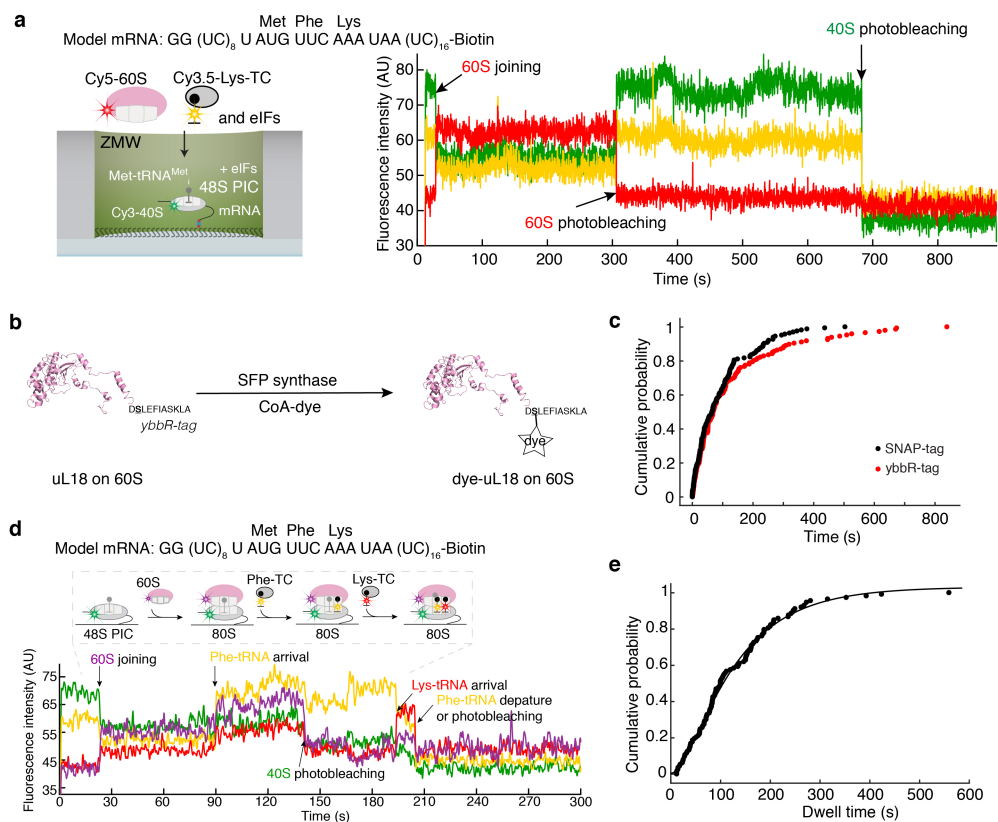
charges or hydrodynamic radius of the complex brought about by the capped mRNA. Both 48S PIC and 80S formation were very inefficient when the cap-binding eIF4F (initiation factors 4A, 4E and 4G) and eIF4B proteins were omitted from the reaction, demonstrating the dependence of initiation on the cap when the full set of initiation factors were added. The experiment was repeated three times with similar results. **c–e**, Using our regime for assembly of the 48S PIC, we would expect the 48S PIC to be in the post-scanning state, with the initiation factors that are required during the scanning process potentially dissociated from the complex. A cryo-EM map at 9.9 Å resolution was obtained for the 48S PIC that formed on the cap-*RPL30* mRNA (grey). This map was compared with previously reported 48S structures<sup>16</sup> in the scanning-competent, mRNA-channel-open configuration (**c**) (EMD 3049; yellow), or scanning-incompetent, mRNA-channel-closed configuration (**d**) (EMD 3048; cyan) (Methods). The cap-*RPL30*–48S PIC was assembled in the same way as for our single-molecule experiments, and the comparisons showed that it resembles the post-scanning closed state, with the Met-tRNA<sup>Met<sub>i</sub></sup> positioned in the P-site (**e**). The modelled Met-tRNA<sup>Met<sub>i</sub></sup> in the EMD 3048 structure, PDB 3JAP, is shown in red.



**Extended Data Fig. 3 | Real-time 80S assembly on the model mRNA at the single-molecule level.** **a**, smFRET assay for subunit joining in ZMWs. 48S PICs were formed by incubating Cy3-40S, Met-TC, model mRNA-biotin, eIF1, eIF1A and eIF5 at 30 °C for 15 min before immobilization in the ZMWs. After washing away free components, the experiment was started with green laser illumination and delivery of Cy5-60S, eIF5 and eIF5B. The reaction was performed in the 1× Recon buffer supplemented with 1 mM GTP:Mg<sup>2+</sup> at 20 °C. **b**, Example experimental trace showing real-time observation of Cy5-60S joining to immobilized Cy3-48S PIC to form the 80S complex, which is identified by the appearance of the smFRET signal. Single photobleaching events are denoted. Similar results were obtained from three independent experiments. **c**, The cumulative probability distribution of the dwell times for 60S joining was fitted to a double-exponential equation, resulting in a fast phase rate of about 0.22 s<sup>-1</sup> with about 46% amplitude, and a slow phase rate of about 0.03 s<sup>-1</sup> with about 54% amplitude ( $n = 178$ ). The kinetics are comparable to previous bulk measurements of the same reaction under similar

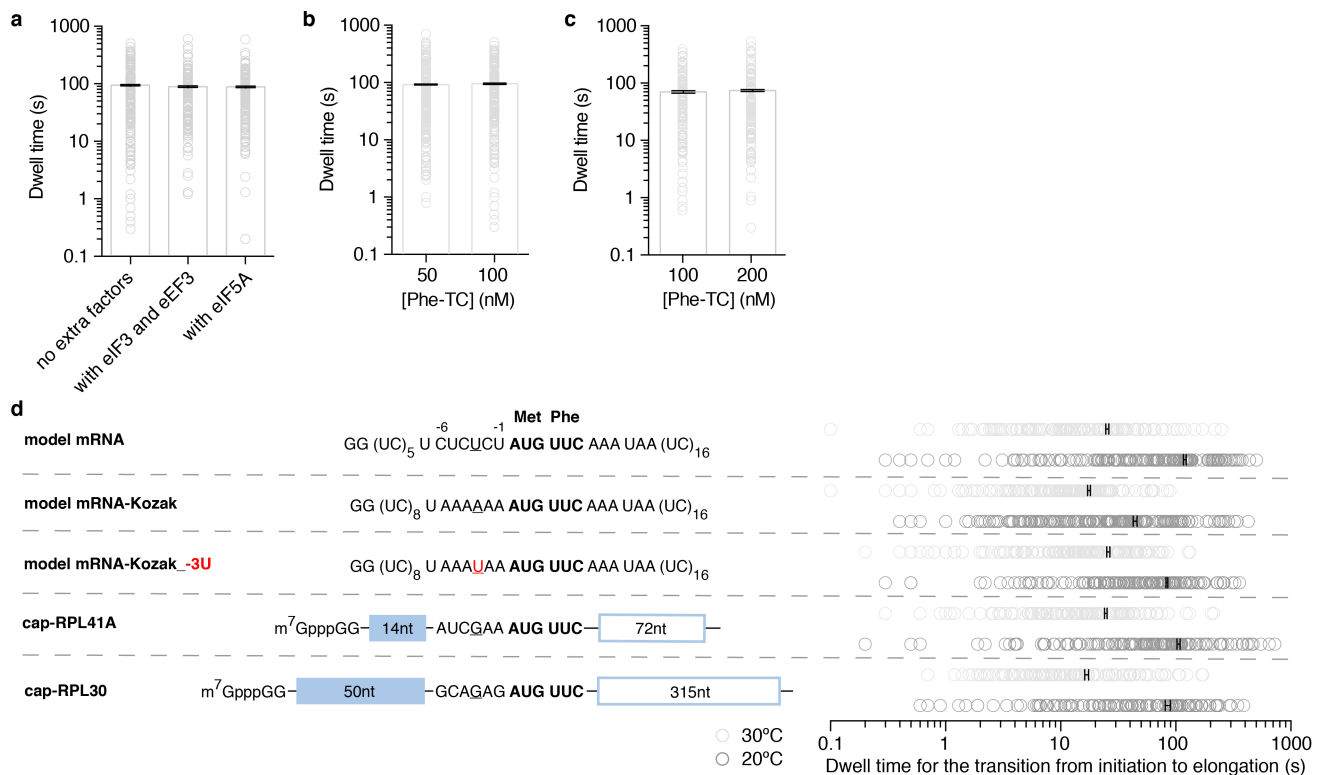
conditions<sup>9</sup> (about 77% fast phase with a rate of about 0.076 s<sup>-1</sup>; about 23% slow phase with a rate of 0.019 s<sup>-1</sup>). **d, e**, Spermidine-driven initiation in the absence of eIF5B. The cumulative probability distributions of the dwell times for 60S joining (**d**) and the transition to elongation (**e**) from experiments performed in the presence or absence of 3 mM spermidine and/or 1 μM eIF5B at 20 °C with the model mRNA were fitted to a double-exponential (**d**) or a single-exponential (**e**) equation. The estimated average fast and slow phase rates ( $k_{fast}$  and  $k_{slow}$ ) and amplitudes ( $A_{fast}$  and  $A_{slow}$ ) of 60S joining (from **d**) and  $\Delta t$  values (from **e**) with the 95% confidence intervals are shown in the inset table in **e**.  $n = 232$  (for addition of spermidine and eIF5B),  $n = 117$  (for addition of spermidine without eIF5B) and  $n = 164$  (for addition of eIF5B without spermidine). Notably, the  $\Delta t$  value is small in the presence of only spermidine—probably owing to the lack of the rate-limiting eIF5B dissociation step. Consistently, this  $\Delta t$  value falls in the same range of the average tRNA arrival times after eIF5B departure in those experiments that were performed with labelled eIF5B (Fig. 2).





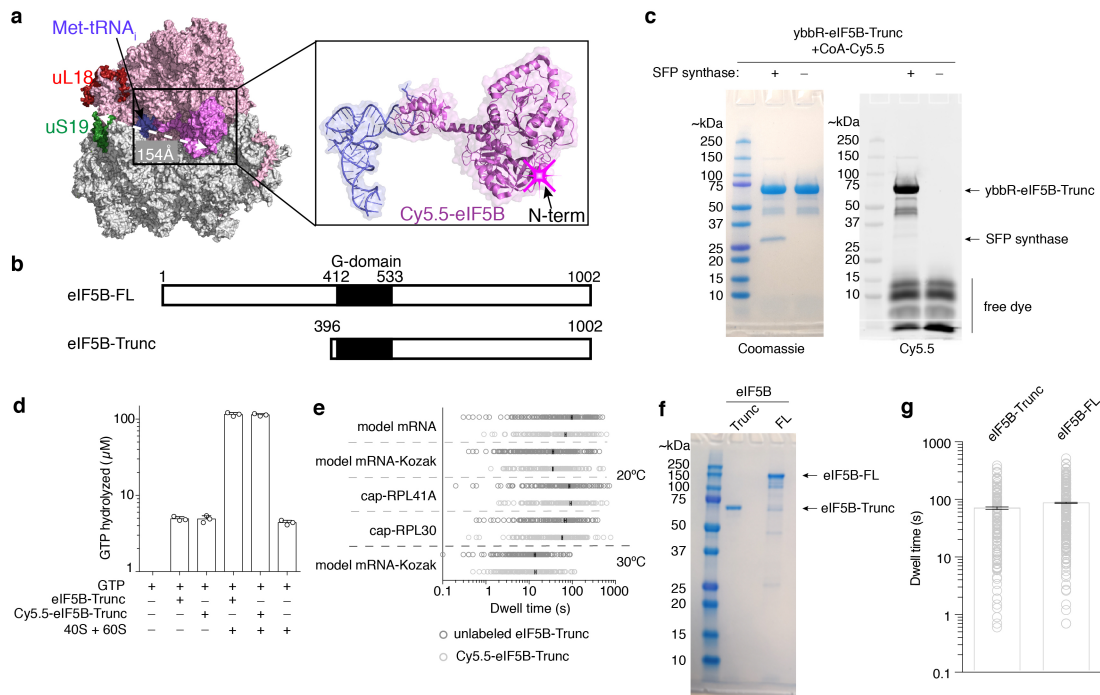
**Extended Data Fig. 4 | Single-molecule assays demonstrate that the association of the first aa-tRNA to the A site is codon- and tRNA-specific and can lead to further elongation.** **a**, Experimental setup (left) and sample fluorescence trace (right) for the single-molecule assay to assess the tRNA-binding specificity of the A site. 48S PICs that contain Cy3-40S, Met-tRNA<sup>Met</sup>, and the 3'-end-biotinylated model mRNA (encoding Met-Phe-Lys-stop) were immobilized in ZMWs in the presence of the required initiation factors. Experiments were started by illuminating ZMWs with a green laser and delivering Cy5-60S, Cy3.5-Lys-tRNA<sup>Lys</sup>:eEF1A:GTP ternary complex (Cy3.5-Lys-TC) and initiation factors. No Cy3.5-Lys-tRNA<sup>Lys</sup>-binding events were observed in the 15-min imaging window, demonstrating that the aa-tRNA association with the A site was codon- and tRNA-specific ( $n = 150$ ). **b-e**, The elongation competence of the 80S complex is scored by smFRET between tRNAs (that is, (Cy3.5)tRNA<sup>Phe</sup>-(Cy5)tRNA<sup>Lys</sup>) after initiation and elongation to the second elongation codon in the model mRNA. To study the tRNA-tRNA smFRET in the context of ribosomal inter-subunit smFRET, we decided to use Cy3 and Cy5.5 to label the 40S and 60S subunits, respectively. Therefore, we engineered the yeast 60S to carry a ybBR tag at the

C terminus of uL18 and labelled the 60S with Cy5.5-CoA by SFP synthase (**b**). **c**, The different tag and label did not notably affect the kinetics of the transition to elongation (red curve,  $\Delta t = 95.4 \pm 2.6$  s (mean  $\pm$  95% confidence interval);  $n = 146$ ; model mRNA, 20 °C and 3 mM free Mg<sup>2+</sup>) compared with the original Cy5-SNAP-tagged 60S (black curve,  $\Delta t = 92.2 \pm 2.5$  s (mean  $\pm$  95% confidence interval);  $n = 164$ ). **d**, Sample fluorescence trace from the experiments in which Cy5.5-60S, Cy3.5-Phe-TC, Cy5-Lys-TC, eEF2, eEF3:ATP, eIF5A and other required initiation factors were delivered to immobilized 48S PICs containing Cy3-40S, Met-tRNA<sup>Met</sup>, and the 3'-end-biotinylated model mRNA, and illuminated with a green laser at 20 °C. Out of  $n = 152$  molecules that showed the sequential 60S and Cy3.5-Phe-tRNA association events,  $n = 113$  molecules showed the subsequent Cy3.5-tRNA<sup>Phe</sup> to Cy5-tRNA<sup>Lys</sup> FRET signal. **e**, The distribution of the dwell times between the appearance of the Cy3.5 and Cy5 signals was fitted to a single-exponential equation, and the average time was  $142 \pm 8$  s (mean  $\pm$  95% confidence interval;  $n = 113$ ). Thus, 74% of the first aa-tRNA associations with the A site yielded the elongation to the next codon.



**Extended Data Fig. 5 | Comparisons of the kinetics of the transition from initiation to elongation under various conditions.** **a–c**, Transition dwell times (open circles) were fitted to single-exponential distributions to estimate the average dwell times (that is,  $\Delta t$  values) (grey bars; error bars in black represent the 95% confidence intervals). **a**, **b**, Comparison of  $\Delta t$  values in experiments performed with the model mRNA at 20°C when no extra factors were added (data taken from Fig. 1d;  $n = 164$ ), or in the presence of eIF3 and eEF3 ( $n = 130$ ) or with addition of eIF5A ( $n = 143$ ) (**a**); or when the concentration of Cy3.5–Phe-TC was 50 nM ( $n = 221$ ) or

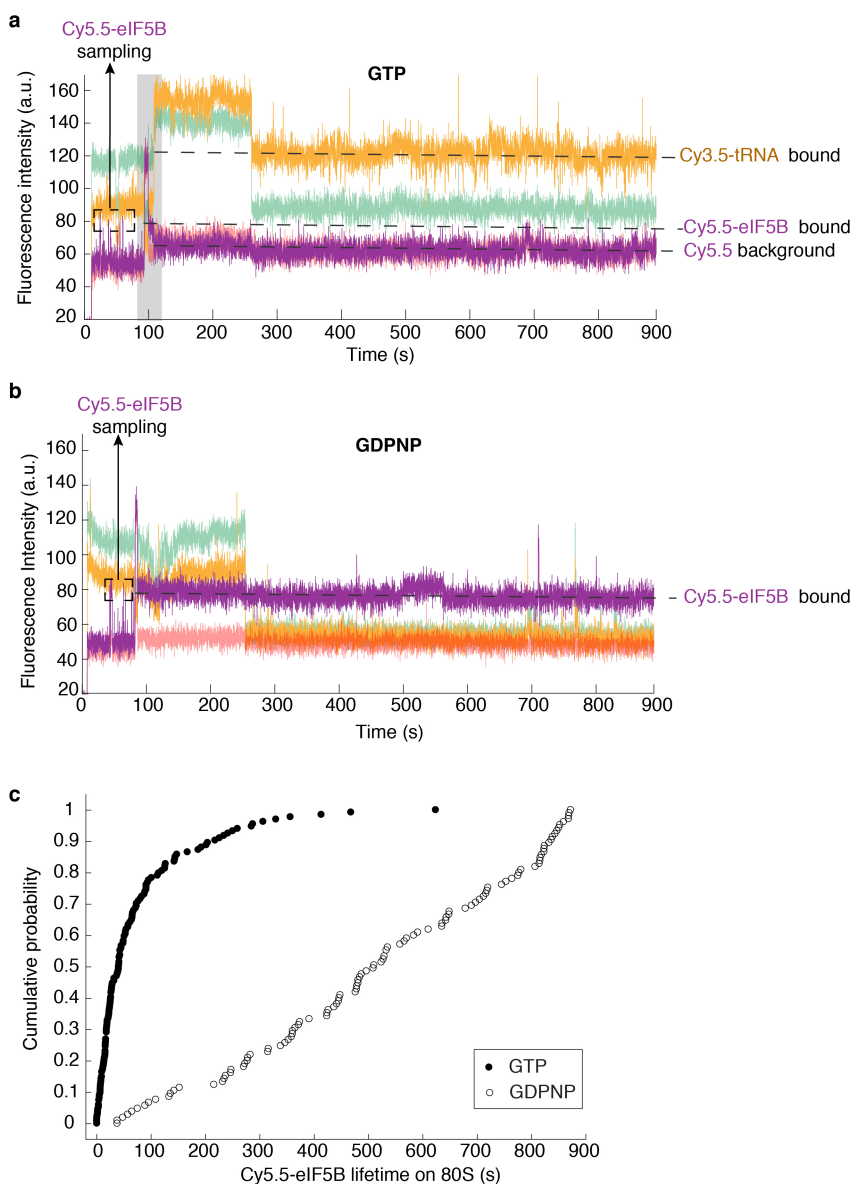
100 nM (data taken from Fig. 1d;  $n = 164$ ) (**b**). **c**, Similar comparison for experiments performed with the cap-RPL30 mRNA at 20°C when the concentration of Cy3.5–Phe-TC was 100 nM ( $n = 118$ ) or 200 nM ( $n = 132$ ). **d**, The  $\Delta t$  values compared across all assayed mRNAs at 20°C and 30°C (Fig. 1a, d). In the model mRNA-Kozak -3U, the A at the -3 position of the optimal Kozak sequence effect. From bottom to top for each group:  $n = 118$ ,  $n = 130$ ,  $n = 130$ ,  $n = 121$ ,  $n = 149$ ,  $n = 161$ ,  $n = 189$ ,  $n = 159$ ,  $n = 164$  and  $n = 136$ .



**Extended Data Fig. 6 | Neither truncation nor fluorescent labelling of eIF5B perturbs its function.** **a**, Fluorescent labelling of eIF5B with Cy5.5 by means of a ybbR tag at the N-terminal end, which is distal from the ribosomal subunit labels and hence not expected to interfere with the inter-subunit smFRET. The ribosome model was created in PyMOL, using data from PDB 4V8Z<sup>12</sup>. **b**, A N-terminally truncated version of eIF5B (eIF5B-Trunc) was used in most of our assays, as in other reported reconstituted, purified yeast translation assays<sup>8,9,11–15,21,25</sup>. Previous reports failed to purify the full-length protein and have demonstrated that the truncated protein supported initiation in vitro and in vivo<sup>8,9</sup>. **c**, We tagged eIF5B-Trunc at the N terminus with a ybbR tag and labelled the protein with a CoA-Cy5.5 dye using SFP synthase. A representative gel is shown, which was first scanned for Cy5.5 fluorescence (right) and subsequently stained with Coomassie blue (left) following SDS-PAGE analysis of ybbR-eIF5B-Trunc after labelling with and without SFP synthase. The experiment was repeated three times with similar results. **d**, The GTPase activity of Cy5.5-eIF5B-Trunc was not perturbed by the labelling. Multiple-turnover GTP hydrolysis was performed in 50 mM HEPES-KOH pH 7.5, 10 mM Mg(OAc)<sub>2</sub> and 100 mM KOAc at 30 °C 30 min before quenching with malachite green assay solution. Where applicable, concentrations were: GTP, 100  $\mu\text{M}$ ; eIF5B-Trunc, 2.5  $\mu\text{M}$ ; Cy5.5-eIF5B-

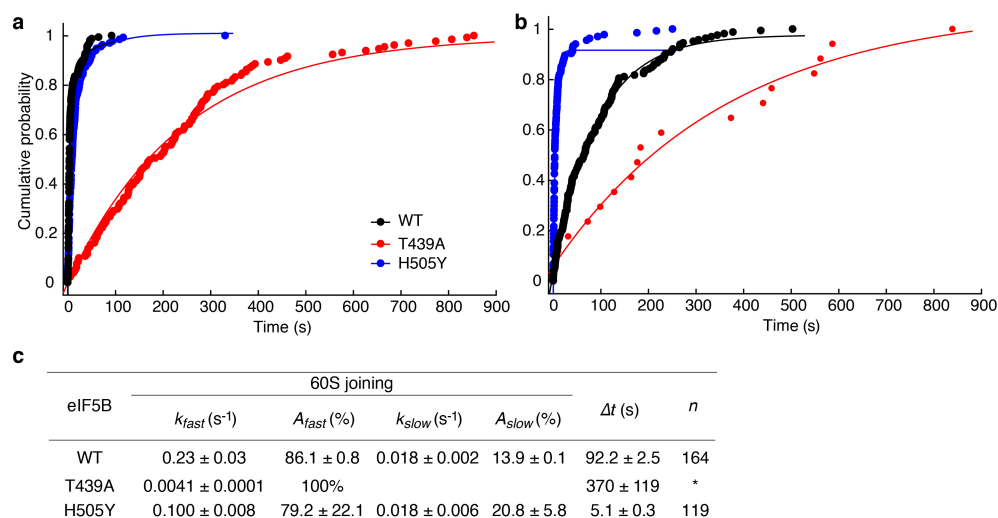
Trunc, 2.5  $\mu\text{M}$ ; 40S and 60S, 0.2  $\mu\text{M}$  each. The GTP-only group was used as a negative control and the values were normalized to 0. Bars represent mean, and error bars indicate standard deviations of three biological replicates (individual data points are indicated with open circles). **e**, The dwell times (open circles) between 60S arrival and the arrival of Phe-TC to the A site were fitted to single-exponential distributions for experiments performed with Cy5.5-eIF5B (related to Fig. 2c) versus those with unlabelled eIF5B (related to Fig. 1d), and at 20 °C or 30 °C. Error bars (in black) represent the 95% confidence intervals of the average dwell times ( $\Delta t$  values). From bottom to top for each group:  $n = 141$ ,  $n = 159$ ,  $n = 164$ ,  $n = 118$ ,  $n = 133$ ,  $n = 130$ ,  $n = 131$ ,  $n = 189$ ,  $n = 134$  and  $n = 164$ . **f**, Despite it being reported previously that purification of recombinant yeast full-length eIF5B (eIF5B-FL) cannot be achieved<sup>49</sup>, we were able to recombinantly express and purify it, as shown by a 12% SDS-PAGE gel analysis. The experiment was repeated three times with similar results. **g**, Use of full-length eIF5B in our assay did not lead to faster transition to elongation in experiments performed with the cap-RPL30 mRNA at 3 mM free Mg<sup>2+</sup> and 20 °C. Error bars (in black) represent the 95% confidence intervals of the average dwell times ( $\Delta t$  values, grey bars) from fitting of the dwell times (open circles) to single-exponential distributions.  $n = 118$  (related to Fig. 1d) (left) and  $n = 205$  (right).





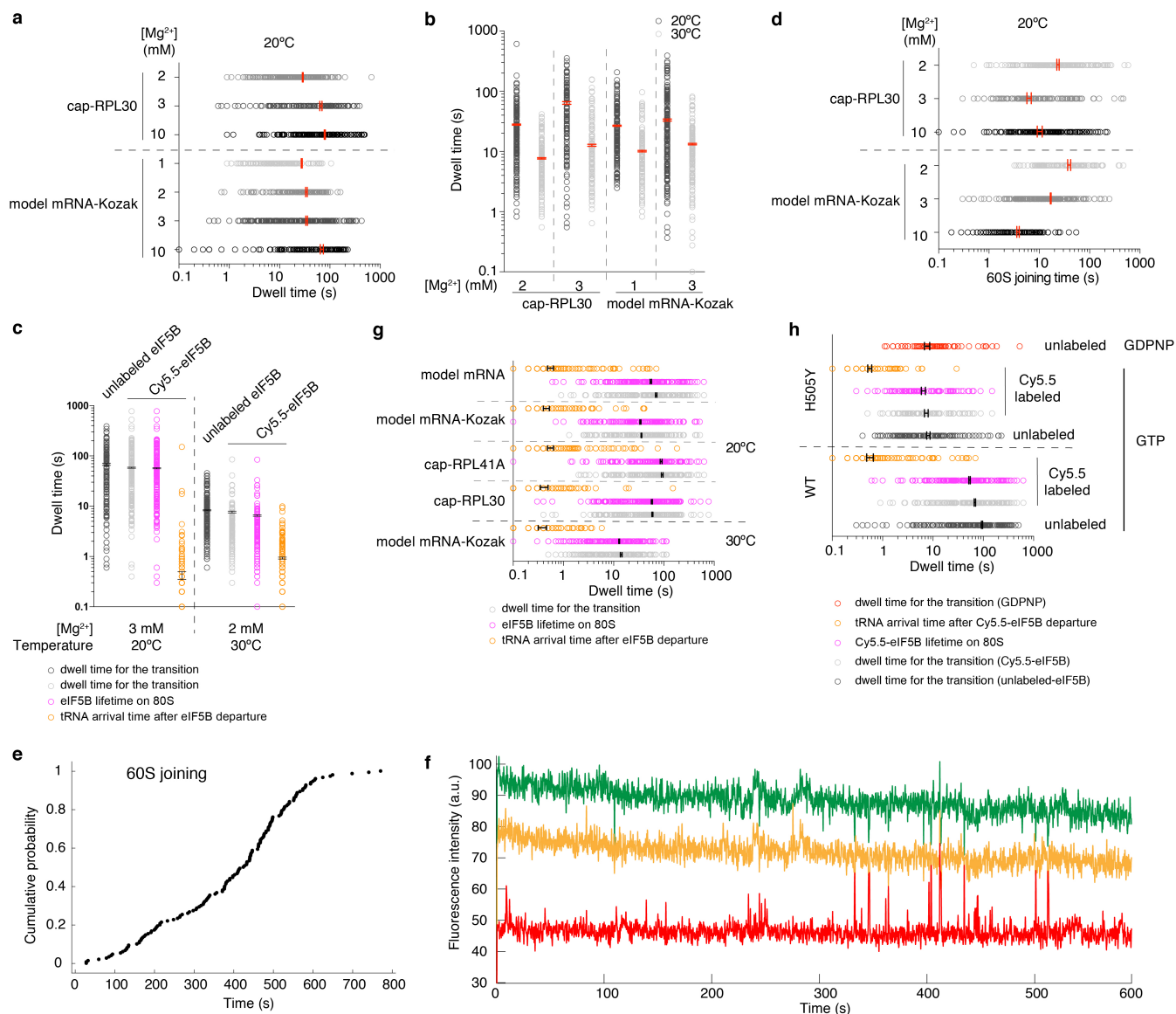
**Extended Data Fig. 7 | Use of a non-hydrolysable GTP analogue, GDPNP, traps eIF5B on the 80S and prevents the transition to elongation.** **a**, Sample trace from experiments performed with GTP ( $n = 134$ ). The grey highlighted part of the trace is shown in Fig. 2a as a magnified view. **b**, Sample trace from experiments performed with non-hydrolysable GDPNP ( $n = 105$ ), in which eIF5B was trapped on the 80S after 60S joining and no tRNA binding to the A site was observed. Black dashed boxes show Cy5.5 events that are transient eIF5B sampling

events to the 48S PIC before 60S joining. **c**, The cumulative probability distributions of the lifetimes of Cy5.5-eIF5B on 80S in experiments performed with the model mRNA at 3 mM  $Mg^{2+}$  and 20 °C in the presence of GTP ( $n = 134$ ; related to Fig. 2d) or GDPNP ( $n = 105$ ). In the presence of GTP, the mean lifetime was 51.9 s ( $\pm 1.8$  s, 95% confidence interval from fitting to a single-exponential equation); in the presence of GDPNP, the mean lifetime was 848 s ( $\pm 19$  s, 95% confidence interval from fitting to a linear equation).



**Extended Data Fig. 8 | The effects of eIF5B mutations on the kinetics of 60S joining and the transition to elongation.** **a, b**, The cumulative probability distributions of the dwell times for 60S joining (**a**) and the transition to elongation (**b**) from experiments performed with unlabelled wild-type eIF5B ( $n = 164$ ), the eIF5B(T439A) mutant ( $n = 131$ ) or the eIF5B(H505Y) mutant ( $n = 119$ ) and the model mRNA at 20 °C in the presence of 3 mM Mg<sup>2+</sup> and 1 mM GTP. **c**, The estimated average fast and slow phase rates ( $k_{fast}$  and  $k_{slow}$ ) and amplitudes ( $A_{fast}$  and  $A_{slow}$ ) of 60S joining (from **a**) and  $\Delta t$  values (from **b**) with the 95% confidence intervals

from fitting the distributions to a double-exponential (wild-type eIF5B and eIF5B(H505Y)) or a single-exponential (eIF5B(T439A)) equation for the 60S joining; or to a single-exponential equation for the transition dwell times. \*In the case of eIF5B(T439A), out of  $n = 131$  molecules showing 60S joining signal, only  $n = 17$  molecules showed the subsequent signal of aa-tRNA association with the A site. Thus, the eIF5B(T439A) mutant is defective in catalysing subunit joining (consistent with bulk measurement<sup>9</sup>), and inhibits tRNA association with the A site.



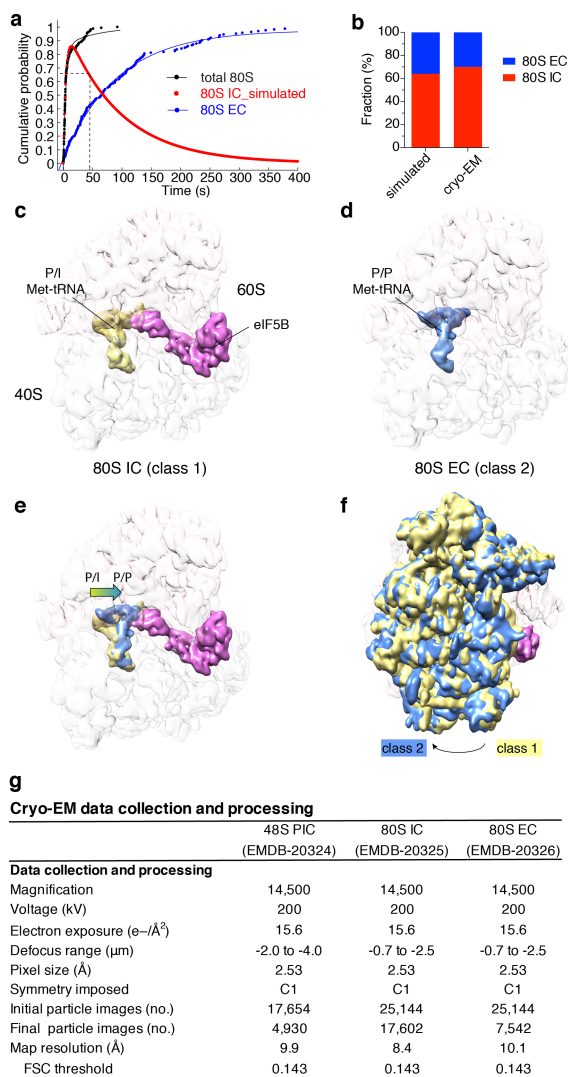
Extended Data Fig. 9 | See next page for caption.

### Extended Data Fig. 9 | Free $Mg^{2+}$ concentration modulates 60S joining and the transition to elongation.

**a**, The dwell times for the transition from initiation to elongation (open circles) were fitted to single-exponential distributions to estimate the average transition dwell times ( $\Delta t$  values, with 95% confidence intervals, red) from experiments performed with unlabelled eIF5B and cap-*RPL30* mRNA or model mRNA-Kozak at 20 °C in the presence of 1–10 mM  $Mg^{2+}$  (data for 3 mM  $Mg^{2+}$  were taken from Fig. 1d). For cap-*RPL30*, unstable 80S formation was observed at 1 mM  $Mg^{2+}$  (f) and thus no  $\Delta t$  values were obtained. From bottom to top for each group:  $n = 108$ ,  $n = 189$ ,  $n = 124$ ,  $n = 150$ ,  $n = 144$ ,  $n = 118$  and  $n = 195$ . **b**, The dwell times for the transition from initiation to elongation (open circles) were fitted to single-exponential distributions to estimate the average transition dwell times ( $\Delta t$  values, with 95% confidence intervals, red) from experiments performed with unlabelled eIF5B and cap-*RPL30* or model mRNA-Kozak, under the indicated conditions. From left to right for each group:  $n = 195$ ,  $n = 152$ ,  $n = 118$ ,  $n = 130$ ,  $n = 150$ ,  $n = 132$ ,  $n = 189$  and  $n = 159$ . **c**, The dwell times (open circles) for the transition from initiation to elongation, eIF5B lifetimes on 80S, and tRNA arrival times after eIF5B departure were fitted to single-exponential distributions to estimate the average dwell times (with 95% confidence intervals, black). Experiments were performed with cap-*RPL30* mRNA at 3 mM free  $Mg^{2+}$  and 20 °C in the presence of unlabelled eIF5B ( $n = 195$ ; data taken from Fig. 1d) or Cy5.5-eIF5B ( $n = 164$ ; data taken from Fig. 2c); or at 2 mM free  $Mg^{2+}$  and 30 °C in the presence of unlabelled eIF5B ( $n = 152$ ; data taken from b) or Cy5.5-eIF5B ( $n = 150$ ). **d**, The dwell times for 60S joining (open circles) from the same experiments as in a were fitted to single-exponential distributions (for model mRNA-Kozak) or double-exponential distributions (for cap-*RPL30*; the average times for the fast phase were plotted here) to estimate the average dwell time (with 95% confidence intervals, red). **e**, The cumulative probability distribution of the 60S joining times, showing the compromised rate of 60S joining in experiments that were performed with the model mRNA-Kozak at 1 mM

$Mg^{2+}$  and 20 °C as in a ( $n = 150$ ). However, we still observed that the arrival of tRNA to the A site occurred readily after 80S formation. The kinetics of 60S joining under these reaction conditions were not fitted well by single- or double-exponential distributions and therefore no average time was deduced for the bar plot in d. **f**, Sample trace from experiments performed with cap-*RPL30* mRNA at 1 mM  $Mg^{2+}$  and 20 °C as described in a ( $n = 200$ ). **g, h**, Dot plots for Fig. 2c, e, showing the single-exponential distributions of the dwell times, with the average dwell times (with 95% confidence interval) in black. Notes: (1) increasing free  $Mg^{2+}$  concentrations increased the  $\Delta t$  values (that is, higher  $Mg^{2+}$  concentration favours the eIF5B-bound semi-rotated 80S conformation (Extended Data Fig. 10)). This seems contrary to the known effects of free  $Mg^{2+}$  concentrations on the conformation of the bacterial pre-translocation 70S elongation complex<sup>50</sup>: lower  $Mg^{2+}$  concentration favours the rotated state and higher  $Mg^{2+}$  concentration favours the non-rotated state. The apparent discrepancy might be a result of the different compositions of the complexes: in our case, the semi-rotated state of the 80S contains an acylated Met-tRNA<sup>Met</sup> in the P site and a protein factor eIF5B bound in the A site; whereas in the pre-translocation 70S complex, the P-site tRNA is deacylated and a peptidyl-tRNA is bound in the A site. The differences in the energy landscape between these two types of complexes can also be explained by the observation that there are no apparent fluctuations between semi-rotated and non-rotated 80S conformations with eIF5B bound, whereas there are frequent fluctuations between rotated and non-rotated 70S conformations in the pre-translocation complexes. (2) The different magnitudes of dependence of  $\Delta t$  values on temperature (Fig. 1d) and  $Mg^{2+}$  concentration for different mRNAs suggest that there are mRNA sequence-context differences in the thermodynamics that govern the transition from initiation to elongation. Similarly, the minimal  $Mg^{2+}$  concentrations required for stable 80S assembly on different mRNAs are different.





### Extended Data Fig. 10 | Cryo-EM analyses of the on-pathway 80S complexes during initiation and the transition to elongation.

**a**, Cumulative probability distributions of the dwell times for 60S joining to 48S PIC (that is, the formation of the 80S complex, which is shown in black and designated as ‘total 80S’) and the subsequent association of aa-tRNA with the A site (corresponding to the  $\Delta t$  value, which is shown in blue and designated as ‘80S EC’) were from the single-molecule experiment with the model mRNA and wild-type eIF5B at 20 °C and 3 mM free  $\text{Mg}^{2+}$  ( $n = 164$ ). The red curve corresponds to the evolution of the fraction of the eIF5B-bound 80S complex (‘80S IC’) over time, simulated with the kinetics of the other two curves. The dashed lines indicate that at time point 45 s, around 64.5% of the 80S complexes should be in the 80S initiation complex state under these conditions. **b**, The population sizes of the two classes of 80S complexes that were observed by cryo-EM (80S IC, 17,602 particles, 70%; 80S EC, 7,542 particles, 30%) were in agreement with predictions from our single-molecule kinetics at time point 45 s. **c–f**, The compositional and conformational differences between the 80S initiation and elongation complexes. **g**, Summary of cryo-EM data collection and processing for the 48S PIC (Extended Data Fig. 2c–e), 80S initiation complex (**c**) and 80S elongation complex (**d**) maps.

## Reporting Summary

Nature Research wishes to improve the reproducibility of the work that we publish. This form provides structure for consistency and transparency in reporting. For further information on Nature Research policies, see [Authors & Referees](#) and the [Editorial Policy Checklist](#).

### Statistics

For all statistical analyses, confirm that the following items are present in the figure legend, table legend, main text, or Methods section.

n/a Confirmed

- |                                     |                                     |                                                                                                                                                                                                                                                            |
|-------------------------------------|-------------------------------------|------------------------------------------------------------------------------------------------------------------------------------------------------------------------------------------------------------------------------------------------------------|
| <input type="checkbox"/>            | <input checked="" type="checkbox"/> | The exact sample size ( $n$ ) for each experimental group/condition, given as a discrete number and unit of measurement                                                                                                                                    |
| <input type="checkbox"/>            | <input checked="" type="checkbox"/> | A statement on whether measurements were taken from distinct samples or whether the same sample was measured repeatedly                                                                                                                                    |
| <input checked="" type="checkbox"/> | <input type="checkbox"/>            | The statistical test(s) used AND whether they are one- or two-sided<br><i>Only common tests should be described solely by name; describe more complex techniques in the Methods section.</i>                                                               |
| <input checked="" type="checkbox"/> | <input type="checkbox"/>            | A description of all covariates tested                                                                                                                                                                                                                     |
| <input checked="" type="checkbox"/> | <input type="checkbox"/>            | A description of any assumptions or corrections, such as tests of normality and adjustment for multiple comparisons                                                                                                                                        |
| <input type="checkbox"/>            | <input checked="" type="checkbox"/> | A full description of the statistical parameters including central tendency (e.g. means) or other basic estimates (e.g. regression coefficient) AND variation (e.g. standard deviation) or associated estimates of uncertainty (e.g. confidence intervals) |
| <input checked="" type="checkbox"/> | <input type="checkbox"/>            | For null hypothesis testing, the test statistic (e.g. $F$ , $t$ , $r$ ) with confidence intervals, effect sizes, degrees of freedom and $P$ value noted<br><i>Give <math>P</math> values as exact values whenever suitable.</i>                            |
| <input checked="" type="checkbox"/> | <input type="checkbox"/>            | For Bayesian analysis, information on the choice of priors and Markov chain Monte Carlo settings                                                                                                                                                           |
| <input checked="" type="checkbox"/> | <input type="checkbox"/>            | For hierarchical and complex designs, identification of the appropriate level for tests and full reporting of outcomes                                                                                                                                     |
| <input checked="" type="checkbox"/> | <input type="checkbox"/>            | Estimates of effect sizes (e.g. Cohen's $d$ , Pearson's $r$ ), indicating how they were calculated                                                                                                                                                         |

*Our web collection on [statistics for biologists](#) contains articles on many of the points above.*

### Software and code

Policy information about [availability of computer code](#)

Data collection

Automated Cryo-EM data acquisition was performed using SerialEM; Single-molecule TIRFM data were acquired using MetaMorph imaging software (Molecular Devices); data from experiments performed on the PacBio RSII instrument were collected using the RSII embedded program.

Data analysis

Single-molecule experimental data were analyzed in MATLAB R2017a (MathWorks) using custom scripts which are available at <https://drive.google.com/drive/folders/1-yKCONui7T7yoJScCuODPhCT4G52emLj?usp=sharing>, and presented figures were prepared in Prism 6 and MATLAB. The Cryo-EM data were processed and visualized using open source softwares: SerialEM, MotionCor2, CTFFIND-4.1, EMAN2, Relion-3.0-beta-2, PyMOL and Chimera (UCSF). Gel images were analyzed using ImageJ 1.50i (National Institutes of Health, USA).

For manuscripts utilizing custom algorithms or software that are central to the research but not yet described in published literature, software must be made available to editors/reviewers. We strongly encourage code deposition in a community repository (e.g. GitHub). See the Nature Research [guidelines for submitting code & software](#) for further information.

### Data

Policy information about [availability of data](#)

All manuscripts must include a [data availability statement](#). This statement should provide the following information, where applicable:

- Accession codes, unique identifiers, or web links for publicly available datasets
- A list of figures that have associated raw data
- A description of any restrictions on data availability

Source data for figures are available as accompanying Source Data files. The cryo-EM maps have been deposited in the Electron Microscopy Data Bank (EMDB) server under the accession codes EMD-20324 (48S PIC), EMD-20325 (80S IC) and EMD-20326 (80S EC). Single-molecule fluorescence trace data are available upon request.

## Field-specific reporting

Please select the one below that is the best fit for your research. If you are not sure, read the appropriate sections before making your selection.

Life sciences       Behavioural & social sciences       Ecological, evolutionary & environmental sciences

For a reference copy of the document with all sections, see [nature.com/documents/nr-reporting-summary-flat.pdf](https://www.nature.com/documents/nr-reporting-summary-flat.pdf)

## Life sciences study design

All studies must disclose on these points even when the disclosure is negative.

Sample size	For all experiments, the number of sample size was chosen on the basis of experimental feasibility, previously established procedures in the lab, and the standards of the field.
Data exclusions	No data were excluded from the analyses.
Replication	All attempts at replication were successful.
Randomization	Samples were not randomized.
Blinding	Experiments were not blinded.

## Reporting for specific materials, systems and methods

We require information from authors about some types of materials, experimental systems and methods used in many studies. Here, indicate whether each material, system or method listed is relevant to your study. If you are not sure if a list item applies to your research, read the appropriate section before selecting a response.

### Materials & experimental systems

n/a	Involvement in the study
<input checked="" type="checkbox"/>	<input type="checkbox"/> Antibodies
<input checked="" type="checkbox"/>	<input type="checkbox"/> Eukaryotic cell lines
<input checked="" type="checkbox"/>	<input type="checkbox"/> Palaeontology
<input checked="" type="checkbox"/>	<input type="checkbox"/> Animals and other organisms
<input checked="" type="checkbox"/>	<input type="checkbox"/> Human research participants
<input checked="" type="checkbox"/>	<input type="checkbox"/> Clinical data

### Methods

n/a	Involvement in the study
<input checked="" type="checkbox"/>	<input type="checkbox"/> ChIP-seq
<input checked="" type="checkbox"/>	<input type="checkbox"/> Flow cytometry
<input checked="" type="checkbox"/>	<input type="checkbox"/> MRI-based neuroimaging